AD-A123 067 A STUDY OF LIQUID JETS(U) ARMY ARMAMENT RESEARCH AND 1/1
DEVELOPMENT COMMAND ABERDEEN PROVING GROUND MD
BALLISTIC RESEARCH LAB G KLINGENBERG ET AL. OCT 82
UNCLASSIFIED ARBRL-MR-03203 F/G 7/4 NL

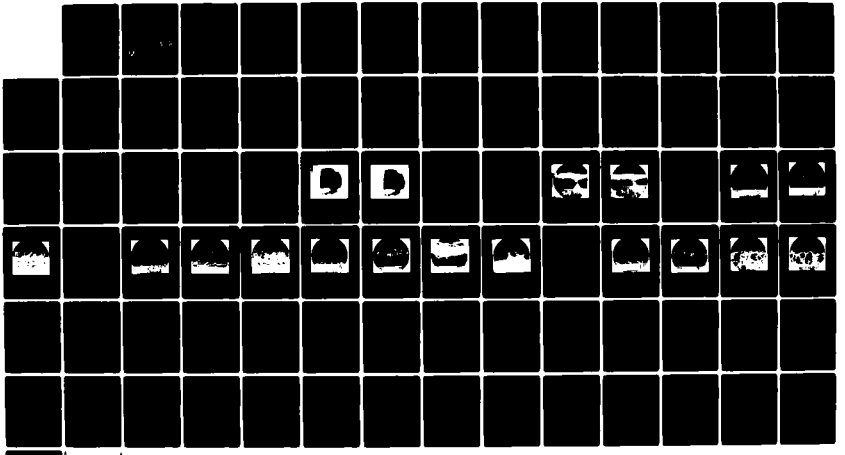

END
DATE FILMED
8-83
DTIC

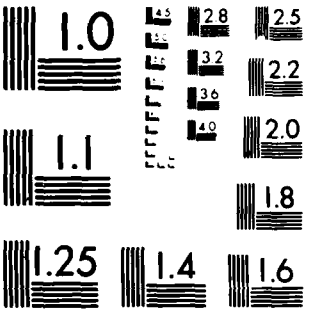

(12)

MEMORANDUM REPORT ARBRL-MR-03203

A STUDY OF LIQUID JETS

Guenter Klingenberg
John D. Knapton
Kenton E. Travis

October 1982

US ARMY ARMAMENT RESEARCH AND DEVELOPMENT COMMAND
BALLISTIC RESEARCH LABORATORY
ABERDEEN PROVING GROUND, MARYLAND

Destroy this report when it is no longer needed.
Do not return it to the originator.

Secondary distribution of this report is prohibited.

Additional copies of this report may be obtained from the National Technical Information Service, U. S. Department of Commerce, Springfield, Virginia 22161.

The findings in this report are not to be construed as an official Department of the Army position, unless so designated by other authorized documents.

The use of trade names or manufacturers' names in this report does not constitute indorsement of any commercial product.

UNCLASSIFIED
SECURITY CLASSIFICATION OF THIS PAGE (When Data Entered)

REPORT DOCUMENTATION PAGE	READ INSTRUCTIONS BEFORE COMPLETING FORM
1. REPORT NUMBER: MEMORANDUM REPORT ARBRL-MR-03203	2. GOVT ACCESSION NO.: AD A123067
	3. RECIPIENT'S CATALOG NUMBER
4. TITLE (and Subtitle): A STUDY OF LIQUID JETS	5. TYPE OF REPORT & PERIOD COVERED: Final
	6. PERFORMING ORG. REPORT NUMBER
7. AUTHOR(s): G. Klingenberg*, J.D. Knapton, and K. Travis**	8. CONTRACT OR GRANT NUMBER(s)
9. PERFORMING ORGANIZATION NAME AND ADDRESS: U.S. Army Ballistic Research Laboratory, ATTN: DRDAR-BLI, Aberdeen Proving Ground, MD 21005	10. PROGRAM ELEMENT, PROJECT, TASK AREA & WORK UNIT NUMBERS: 1L161102AH43
11. CONTROLLING OFFICE NAME AND ADDRESS: US Army Armament Research & Development Command, US Army Ballistic Research Laboratory (DRDAR-BL), Aberdeen Proving Ground, MD 21005	12. REPORT DATE: October 1982
	13. NUMBER OF PAGES: 82
14. MONITORING AGENCY NAME & ADDRESS (if different from Controlling Office)	15. SECURITY CLASS. (of this report): UNCLASSIFIED
	15a. DECLASSIFICATION/DOWNGRADING SCHEDULE

16. DISTRIBUTION STATEMENT (of this Report)

Approved for public release; distribution unlimited

17. DISTRIBUTION STATEMENT (of the abstract entered in Block 20, if different from Report)

18. SUPPLEMENTARY NOTES

*Fraunhofer-Institut Fuer Kurzzeitdynamik, Ernst-Mach-Institut Abteilung Fuer Ballistile (EMI-AFB), Haupstrasse 18, 7858 Weilam Rhein, West Germany
**Deceased

19. KEY WORDS (Continue on reverse side if necessary and identify by block number)

20. ABSTRACT (Continue on reverse side if necessary and identify by block number)

raj

Various correlations were examined that have been used in the past for predicting mean droplet sizes generated by a single fluid jet. The correlation were compared with semi-quantitative data obtained from spark photographs and from a particle sizing interferometer. Jet properties were investigated for three types of fluids, i.e., water, Hexane, and a moderately energetic liquid monopropellant (LP) used in gun applications. The photographic data are only suitable for a semiquantitative analysis due to severe

DD FORM 1 JAN 73 1473 EDITION OF 1 NOV 65 IS OBSOLETE

UNCLASSIFIED
SECURITY CLASSIFICATION OF THIS PAGE (When Data Entered)

Abstract (Cont'd):

20. diffraction problems. Some preliminary low velocity droplet data were obtained with the particle sizing interferometer. The results strongly suggest that all correlations overestimate the droplet size and that the best agreement was obtained from a theoretical analysis by Mayer. Some additional studies were also performed on frictional heating and droplet scattering by an electric field. No evidence of ignition of the liquid monopropellant (LP) from frictional heating was found. Some evidence of droplet scattering by the electric field could be inferred from the photographs.

TABLE OF CONTENTS

RE: Classified Reference, Distribution Unlimited
No change per Mr. Paul Ryan, BRL/DRDAR-TSB-S

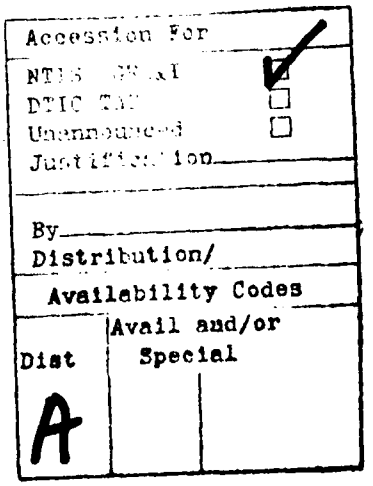

LIST OF ILLUSTRATIONS

LIST OF ILLUSTRATIONS (Continued)

LIST OF TABLES

I. INTRODUCTION

The study of fluids ejected from nozzles and the breakup of the fluid jet into droplets have been investigated for over a century. In recent decades ejected fluids have found application in numerous areas such as fuel injection studies for heat and power generation,automotive and jet fuel injection, rocket chamber propellant injection, paint and insecticide sprayers and, recently,high speed printers. Also, more recently, interest has been revived in an ejected fluid method for controlling the combustion of liquid propellants in guns. The method is called regenerative injection and is the motivation behind this study.

The present study was formulated to establish a basis for characterizing liquid monopropellants used for gun applications when ejected into one atmosphere and to incorporate sufficient design flexibility to permit later studies at higher ambient pressures. The objectives of the study include investigations of: (1) jet breakup at one atmosphere using various fluids ejected from a simple hole nozzle and (2) correlations in droplet size and fluid properties suitable for engineering gun models. In addition, two related investigations were undertaken during the program which included studies on both the effect of an electric field on the jet during injection and on possible propellant ignition due to frictional heating under high speed flow conditions. Fluids that have been tested are water, Hexane, and a moderately energetic liquid monopropellant (LP) used in gun applications.

Objectives (1) and (2) are concerned with an evaluation of correlations suitable for use during the ignition interval of regenerative injection gun models. The data obtained for the evaluation can also provide quantitative guidelines on jet breakup and droplet size. Data characterizing the dynamics of the injection process is of fundamental importance since it is known from rocket engine investigations that the injection process can be a primary source of instabilities during both the ignition and combustion phases.

The study on the effect of an electric field is of interest as a method for decreasing droplet size during the early low pressure injection stage. For gun applications it was postulated that the injection of smaller liquid propellant droplets during the start-up of the regenerative injection process would enhance the ignition and result in a more smooth build-up in pressure. The study on frictional heating is related to problems that might occur during rapid propellant loading or problems with possible leakage around moving components, especially under

gun pressure conditions.

Forming a background for the study are the numerous reviews on fluid jet research that have been conducted over the years. In particular, the following reviews are noted: Putnam et. al. (1957)[1], Forsnes and Ulrich (1968)[2], Harrje and Reardon (1972)[3], Jones (1977)[4], and Faeth (1977)[5]. References 1 and 3 are comprehensive literature reviews, the former including summaries of the important early work. The latter is a more critical review and offers an introduction to the subject of combustion instabilities in rocket motors. Reference 2 is a summary of droplet formation mechanisms and provides a review of various droplet correlations. Reference 4 is a review of various techniques, including an interferometer which was selected for use during these studies. Reference 5 is a general review of fluid jet and droplet characteristics including combustion effects.

Before proceeding to describe these studies, a review on the background summarizing the behavior of a jet when emerging from a nozzle and, also, of various droplet correlations will be given. For comparison purposes, the review will include calculations of the fluid jet and of droplet characteristics for the three different fluids at two arbitrarily selected velocities; namely, 10 m/s and 100 m/s. Although the ejection velocities are arbitrary, they provide a basis for comparing correlations with the preliminary results summarized later in the report. The physical properties of the fluids tested are given in Table I; constant values are tabulated, although it is recognized that an accurate description of the fluid jet breakup phenomena would likely require information on the time dependent fluid properties. The wall shear values listed in Table I are based on the product $\rho^{3/4}\ \mu^{1/4}$, according to the analysis of Janna and John [7], and represent the wall shearing effects relative to water for constant flow and nozzle geometry.

Table I. Physical Properties of Fluids

Fluid units	Density ρ kg/m³	Surface Tension σ N/m	Viscosity μ Ns/m²	Normalized wall shear τ -	Critical Temperature T_c K	Critical Pressure P_c MPa	Reference
Water	1000	0.0727	0.0010	1.00	647	21.8	6
Hexane	659	0.0184	0.00032	0.55	508	3.0	6
LP	1400	0.054	0.00745	2.3	-	-	-

II. BACKGROUND

A. Jet Breakup

The stability of a jet ejected from a nozzle depends on many factors and an accurate description of the flow from an orifice involving complex flow patterns is best studied from a combined detailed experimental and theoretical approach. The effects of turbulence in the nozzle, nozzle geometry, and interactions with a turbulent gas are difficult problems that can readily introduce flow disturbances and hydrodynamic instabilities. For example, Grant and Middleman[8] report on studies by other researchers who claimed turbulent jet flow was initiated at Reynolds numbers varying from 240 in one paper to as high as 10 000 in a different paper. They state further that a single value for the Reynolds number corresponding to the breakdown of laminar flow is not likely for nozzle l/d ratios of less than 5 or 10. Lafrance and Ritter[9] describe the details of one design using a conically shaped section between a "quieting chamber" and a glass tube which yielded laminar jets at Reynolds numbers up to 8000.

As a simplifying approach for the present study, a circular cross section nozzle was selected. This type of nozzle yields a relatively simple flow pattern and has been studied extensively. Correlations will be reviewed to permit comparison with the preliminary data summarized later in the report. Before examining the correlations, a brief description of fluid jets will be given.

A fluid jet ejected from the nozzle may be characterized by an L-v plot where L is the jet breakup length and v is the jet velocity. Such curves are described by Grant and Middleman[8] and later by Newmann and Brzustowski[10]. They show a monotonic increase to a first maximum in L. The increase in L up to the first maximum is laminar and is reasonably well predicted by the early theory of Weber as reviewed by Grant and Middleman[8]. The first maximum in L is associated with the onset of turbulence. Further increase in the jet velocity results in a decrease in L to a minimum[10]. The curve then reverses and continues to a second maximum in L which determines the transition from primary to secondary atomization. Primary atomization is a result of jet breakup due to the growth of capillary instabilities on the surface which produce relatively large globules. The globules may further breakup due to aerodynamic forces. Secondary atomization is due to the stripping or shearing of liquid globules and droplets from the jet surface. For the case of secondary atomization, the globules will likely disintegrate into smaller droplets, again depending on the aerodynamic forces.

Many studies have been made attempting to characterize the L-v region based on the fluid dynamic parameters associated with the jet. Some of the more relevant parameters are listed in Table II which includes values for the Reynolds number, Weber number, Laplace number, and Ohnesorge number of the three test fluids at the two selected velocities of 10 m/s and 100 m/s. The Reynolds number R_e represents the ratio of the fluid dynamic pressure (ρv^2) to the viscous stress ($\mu v/D$). The Weber number W_e represents the ratio of the aerodynamic pressure ($\rho_g v^2$) to the surface tension pressure (σ/r). The Laplace number L_p is proportional to the ratio of the surface tension pressure to the viscous stress multiplied by the Reynolds number R_e resulting in a term independent of velocity. Finally, the Ohnesorge number O_e, also independent of velocity, is proportional to the ratio of the square root of the Weber number W_e to the Reynolds number R_e .

Table II. Summary of Various Dimensionless Ratios Characterizing Fluid Jets Emerging into one Atmosphere from a 1.6 mm Orifice

Velocity	Fluid / Number	R_e $\frac{D\rho v}{\mu}$	W_e $\frac{r\rho_g v^2}{\sigma}$	L_p $\frac{D\rho\sigma}{\mu^2}$	O_e $\frac{\mu}{\rho}\left(\frac{\rho}{\sigma r}\right)^{1/2}$
10 m/s	Water	1.6×10^4	1.3	1.1×10^5	7.1×10^{-5}
100 m/s		1.6×10^5	130		
10 m/s	Hexane	3.3×10^4	5.2	1.9×10^5	6.9×10^{-5}
100 m/s		3.3×10^5	518		
10 m/s	LP	3.0×10^3	1.8	2.2×10^3	4.4×10^{-4}
100 m/s		3.0×10^4	177		

An interesting feature of the Laplace number L_p is the dependence of $L_p^{-1/2}$ on R_e as discussed by Borodin et al.[11] who reviewed the work of Ohnesorge (1937) and Littaye (1939). Using the values of R_e and $L_p^{-1/2}$ in Table II, and comparing with Ohnesorge's plot of $L_p^{-1/2}$ vs. R_e shows that the fluid jets under study will fall into the jet surface wave disintegration region for the arbitrarily selected velocity of 10 m/s and into a jet atomization region at 100 m/s. Also, the values associated with

Hexane, when compared with the other two fluids, result in shifting the jet breakup further into the atomization region. It must be emphasized that with special precautions in fabricating the nozzle as mentioned by Lafrance and Ritter[9] or if protuberances are present in the flow field, then the jet breakup regions for the three test fluids would shift back into the atomization region or into the jet surface breakup region, respectively. Interestingly, however, the shift into the breakup region according to Borodin et al.[11] still retains a linear dependence on a $L_p^{-1/2}$ vs. R_e log-log plot.

The significance of the Ohnesorge number O_e is based on a review by Grant and Middleman[8]. Their review suggested a possible correlation between O_e and the first maximum in the L vs. v plot (breakup length vs. velocity).

Considering the high Reynolds numbers associated with the jets in the present study, we conclude that the jets will likely exist in a turbulent region where disintegration is mainly due to an atomization process, especially for the higher velocity jets of Table II.

While commencing these studies, it was considered that one of the more readily measured parameters would be the jet breakup length L. From the discussions of the different regions in the L vs. v plot, various jet breakup lengths L might be expected depending on the velocity v. Rice[12] in Reference 3 reviewed the low velocity region which is characterized by a jet breakup process dependent on capillary forces (surface tension effects). For the low velocity case, the jet breakup length as derived by Weber[12] is

$$L = v \left[(8\rho r_j^3 / \sigma)^{1/2} + 6\mu r_j / \sigma \right]. \qquad (1)$$

Assume as in Table II a jet diameter as it emerges from the nozzle of 1.6 mm and a jet velocity of 10 m/s. For the three test fluids only the first term in Eq (1) need be considered. Values for L are 75 mm, 108 mm, and 120 mm for the fluids water, LP, and Hexane.

For the high velocity region and based on an energy balance analysis of Levich, also outlined in the review by Rice[12], L may be approximated by

$$L = v \, r_j \, (\rho_l / \rho_g)^{1/2}. \qquad (2)$$

The analysis assumes a low viscosity fluid. The same expression for L is found assuming either a short wavelength disturbance on the jet (atomization) or a long wavelength disturbance (large drop size fragmentation). At a jet velocity of 100 m/s, values for L are 23 mm, 27 mm, and 19 mm for the test fluids water, LP, and Hexane.

B. Droplet Studies

The breakup of the fluid jet into drops is required for liquid propellant gun application in order to achieve an adequate mass burning rate. Aside from the early start-up phase during ignition, the breakup of the fluid jet into sufficiently small droplets is assured due to the injection velocities and the selection of an appropriate orifice diameter. The droplet sizes may cover a considerable range and for a comprehensive analysis a droplet distribution function would have to be determined. Such functions have been considered by Mugele and Evans[13], Groeneweg[14], Lekic et al.[15], Simmons[16], Sato and Sakai[17], and Janna and John[7]. For the present study, only the mean droplet correlations will be examined.

Many droplet correlations have been proposed[2] for examining both the low velocity region where the jet breaks up into relatively large fragments, and a high velocity region where the jet disintegrates due to atomization or surface stripping into very small drops. Some of the correlations, considered appropriate to this study, are summarized and calculated droplet values, where appropriate, are given in Table III for the three test fluids at the two arbitrary velocities of 10 m/s and 100 m/s. It should be recognized that the appropriateness of a calculated droplet value must depend on the applicable velocity region which is indicated at the top of each column in Table III. Droplet values for the two velocity regions are included for comparison purposes.

First, a droplet size calculation is given for the low velocity limiting case based on the analysis of Weber (reviewed in Reference 12). The analysis is independent of velocity and is based on a jet breakup due to an increase in amplitude of a wavelength disturbance on the jet surface.
From Reference 12

$$D = 1.88\ d_j \left[1 + \frac{3\mu}{\sqrt{\rho\ \sigma\ d_j}} \right]^{1/6}. \qquad (3)$$

For the three fluids under consideration the term in the brackets only has a negligible effect on d_1.

One of the more widely used correlations that were applied during early fuel injection studies[18] is the Weber number, referred to earlier. This ratio offers a simple approach for estimating droplet sizes; however, the usefulness of the method was considered inadequate in two studies (quoted in Reference 2) performed by Hanson et al. (1963) and Rabin et al. (1964). These authors further concluded that a critical W_e number is required to determine droplet breakup and that different W_e numbers would be required depending upon the relative velocity between the gas and liquid. Because of these uncertainties, the applicability of the W_e number must be limited when attempts are made to estimate the droplet size.

TABLE III. Values of Exponents on Physical Properties Based upon Various Droplet Studies, (The Droplet Sizes are Calculated for Velocities of 10 m/s and 100 m/s for the Three Test Fluids with a Jet Diameter of 1.6 mm)

PHYSICAL PROPERTIY / STUDY	WEBER[12]	WEBER NUMBER[2] (a)	WEISS and WORSHAM[19]	MAYER[20]	NUKIYAMA and TANASAWA[21-23]	DOMBROWSKI and HOOPER[24]	WOLFE and ANDERSON[25]	PRESENT STUDY
	(Low velocity limiting case)	(Both low and high velocity, dep. on W_e crit) (b)	(High velocity, empirical)	(High velocity, theoretical)	(Velocity subsonic, empirical) (c)	(Sheet spray, low velocity, theoretical)	(High velocity, theoretical)	
μ_l	1/6	0	1/3	2/3	0	0	1/3	1/3
σ_l	-1/12	1	5/12	1/3	1/2	0.2	1/2	1/3
ρ_l	-1/12	0	-5/6	-1/3	-1/2	-0.65	-1/6	-3/4
ρ_g	0	-1	0	-2/3	0	1/4	-2/3	1/4
v	0	-2	-5/4	-4/3	-1	-0.8	-4/3	-1
d_j	11/12	0	1/6	0	0	0	1/6	1/3
FLUID			DROPLET SIZE(μm)					
WATER								
v = 10 m/s	3010	1210	1420	370	500			
v = 100 m/s		45	73	17	50			
HEXANE								
v = 10 m/s	3010	1530	680	125	309			
v = 100 m/s			35	6	31			
LP								
v = 10 m/s	3040	--	2130	1130	363			
v = 100 m/s			108	53	36			

a: $D = \sigma / \frac{W_e \text{ crit}}{\rho_g v^2}$; b: see text for W_e crit; c: second term omitted, see text

For illustrative purposes, the droplet sizes indicated in Table III for water are based on critical Weber numbers of 2.0 and 7.5 at v = 10 m/s, and 100 m/s, respectively. These values were obtained by extrapolating on a linear plot the critical Weber numbers for water summarized in Reference 2. (Critical Weber numbers taken from Reference 2 for water and Methyl Alcohol are given in Appendix A).

A droplet size is also given for Hexane based on a critical W_e number of five and a jet velocity of 10 m/s. The value of five was selected using a linear extrapolation of the data summarized in Reference 2 (see also Appendix A), in this case for Methyl Alcohol which has a surface tension about 9% greater than that for Hexane (the viscosity for Methyl Alcohol is about 1.8 times larger). The maximum velocity in Reference 2 for Methyl Alcohol was 47.9 m/s and did not warrant a calculation of the droplet size for a velocity of 100 m/s.

No droplet sizes are given for the other conditions indicated in Table III since no information was found suitable for estimating an appropriate critical Weber number.

The discussion on the Weber number by Forsnes and Ulrich in Reference 2 concludes with a summary of attempts, made by Hanson et al. 1963, to correlate the critical Weber number with viscosity. Forsnes and Ulrich state that Hanson, Domich, and Adams "found that the critical Weber number was not constant for liquids of approximately the same viscosity, but that it increased with decreasing diameter for each of the experimental liquids" as indicated by the data in Appendix A.

An empirical study by Weiss and Worsham[19], consisting of 101 tests using three different injectors, three different liquids and injections both axial and transverse to an air stream, resulted in the formulation of a group of dimensionless terms which yielded, when solved for the droplet diameter,

$$D \sim \frac{\sigma}{\rho_g v^2} \left(\frac{v\mu}{\sigma} \right)^{2/3} \left(1 + \frac{10^3 \rho_g}{\rho_l} \right) \left(\frac{W \rho_l \sigma \mu_g}{\mu_l^4} \right)^{1/12} \qquad (4)$$

where the proportionality constant was found to be 0.61. Weiss and Worsham[19] state that the standard deviation of the entire group was 25 %, however, the correlation was improved by disregarding nine of the tests with $W_e < 25$ which included some of the tests with their smallest (1.2 mm) injector. A summary of the exponential dependencies established by Weiss and Worsham and the calculated droplet sizes are listed in the fourth column in Table III. For purposes of calculation, and based on the experimental studies described later, W was set equal to 0.05 kg/s

and 0.15 kg/s for v = 10 m/s and 100 m/s, respectively.

The study by Mayer[20], shown in the fifth column of Table III, is based on an analysis of surface capillary instabilities and yielded

$$D \sim \left[\frac{\mu \ (\sigma/\rho)^{\frac{1}{2}}}{\rho_g \ v^2} \right]^{\frac{2}{3}}. \qquad (5)$$

Mayer indicated that the proportionality constant, with some theoretical justification, was approximately 21.4.

A second empirical correlation for droplets generated by a gas atomizing nozzle is listed in Table III based on early studies by Nukiyama and Tanasawa [21-23]. (Reference 22 contains a listing of translations of the original articles.) The authors showed that

$$D = \frac{0.585}{v} \sqrt{\frac{\sigma}{\rho}} + 0.00168 \left(\frac{\mu}{\sqrt{\sigma \rho}} \right)^{.45} \left(1000 \frac{Q_l}{Q_g} \right)^{1.5} \qquad (6)$$

where v is subsonic (m/s)

$0.019 < \sigma < 0.073$ N/m

$700 < \rho < 1200$ kg/m^3

$0.0003 < \mu < 0.05$ N s/m^2

Q_l/Q_g = ratio of liquid volume to gas volume.

The ratio Q_l/Q_g is usually sufficiently small[21,23] so that the second term in Eq (6) may be neglected, as in the calculations shown in Table III.

Correlations from two additional studies are also summarized in the seventh and eighth columns of Table III, although no droplet calculations are given, as these correlations are not considered appropriate for the present study. They are included here for comparison purposes to illustrate the general agreement between the exponents associated with the various parameters.

The correlation of Dombrowski and Hooper[24] is based on an analysis that describes the wave growth on a fan type of spray jet. Their final equation is empirically adjusted based on actual data. Equations for fan spray jets are not considered applicable to the present study. Nevertheless, it is interesting to note the agreement between the exponential dependencies with the other studies.

The correlation of Wolfe and Anderson[25] considers a different approach and is based on a rate process theory. Their final equation requires a curve fitting procedure to determine two constants and is not readily suitable for calculations since informations on the droplet size is required prior to breakup. The agreement among the exponential dependencies, however, is again noted.

The last column in Table III is the result of a dimensional analysis which can be obtained formally by simply multiplying the W_e number, the reciprocal of the R_e number, and the ratio of the gas density to the liquid density.

III. EXPERIMENTAL

A. Background

The liquid jet required for the studies was generated using equipment obtained from an earlier jet study at the BRL[26].

The methods selected for characterizing the jet and droplets consisted of high speed photography and an optical sizing interferometer. Forming the basis for the photographic set-up were studies by Seebaugh and Lee[27] and Matthews, Wuerker and Harrje[22], who investigated various optical methods for observing the breakup of jets. Seebaugh and Lee[27] selected for most of their studies a short exposure (10 μsec) shadowgraph technique. A similar set-up, but with a shorter duration spark (< 1 μsec), was used in the present study. It was recognized that the pulsed laser techniques described in Reference 22 might offer improvements in the quality and resolution in the photographs over what might be possible with a spark system. However, the spark system was selected due to its immediate availability, lower cost and our consensus that the photographs obtained with the spark system would at least provide a semiquantitative characterization of the jets.

The selection of an optical sizing interferometer for measuring the droplet sizes was based on the work of Farmer [26,30] and review articles by Hong and Jones[31], Jones[32], and Robards[33]. More recent studies by Farmer et al.[34], McComb and Salch[35], Wigley[36], Thorn et al.[37], and Bachalo[38] further demonstrate the applicability of the method.

B. Liquid Jet System

A fast opening valve system, shown in Figure 1, was selected for applying a pressure step to a differential area piston. Operation of the system was described in References 26,39. Briefly, the Valve Head is first seated in the Head Chamber. The chamber is then pressurized with Nitrogen gas. The actual injection pressure applied to the jet is based on the pressure level in the Head Chamber multiplied by the differential area ratio of the piston in the Head Chamber to the area of the Injection Piston. About 3 cm^3 of liquid was used for the tests, although the amount can be varied depending on the location of the housing for the Injection Piston. The jet was fired by applying pressure to the Firing Chamber which results in an increasing pressure on the rear piston of the Valve Stem. The Valve Stem is elastically stretched until the force on the Valve Head plus frictional retarding forces are overcome at which time the entire Valve Stem snaps back (to the left in Figure 1) resulting in a pressure step on the differential area piston. The force on the differential area piston is transmitted to the Injection Piston which is displaced forward ejecting the fluid. Motion of the Injection Piston was monitored in the early tests using a linear position transducer, although this was abandoned in the later tests for convenience and due to the reliability of the system. An adjustable electrical contact was attached to the Injection Piston and provided a means for triggering other events, such as a spark light source, at any desired time during the injection. Motion of the Injection Piston and the trigger event were recorded on a dual beam oscilloscope. For most of the tests the trigger event was set at one-half of the displacement of the Injection Piston.

Tests were run using Nitrogen gas in the Head Chamber at pressures of 0.34 MPa, 0.69 MPa, 3.45 MPa, and 6.9 MPa. The volume of the Head Chamber is sufficiently large so that the pressure drop during injection is less than one percent. Motion of the Injection Piston was generally linear with time except for a few tests which indicated an initial velocity less than the average velocity.

C. Electrode System

The electrode system consisted of two polished parallel steel plates, 50 x 75 mm, separated by 24 mm, and centered about the axis of the jet. The center of the plates was 75 mm from the nozzle.

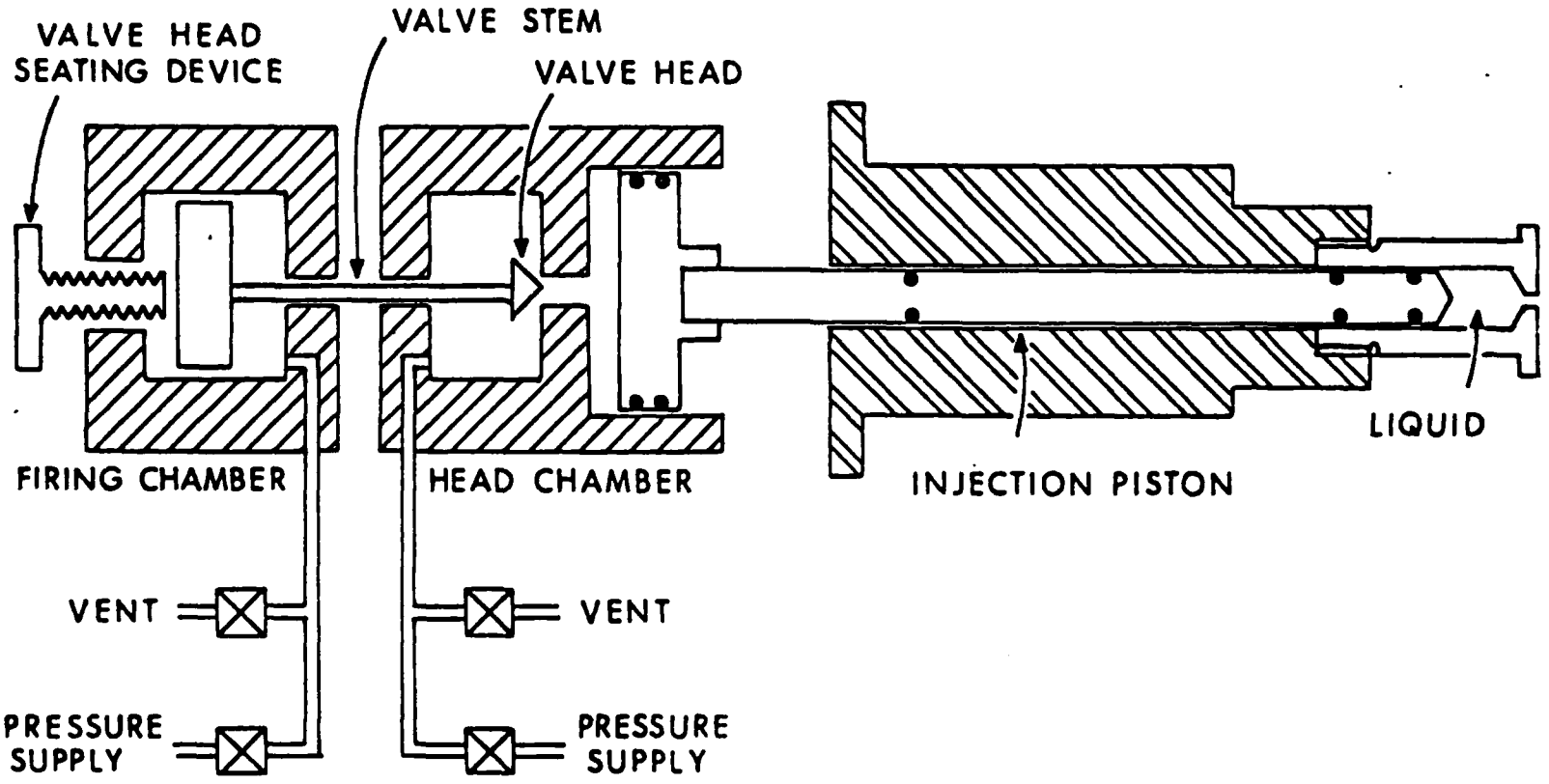

Figure 1. Fast Opening Valve System Used for Generating a Liquid Jet

D. High Speed Photographic Set-up

Two approaches were used for obtaining information on the jet and droplet characteristics. Both approaches consisted of a shadowgraph type of set-up. In the first approach, shown in the upper diagram in Figure 2, the jet was backlighted as illustrated. The light source was an EG&G model 501 high speed stroboscope with a minimum flash duration between one to two μs. The unit was operated at its highest flash rate of 5000 Hz which was synchronized with a Hycam camera. The film was 35 mm Ektachrome 7242 for use with high speed cameras. The framing rate provided a basis for estimating the jet velocity as well as viewing the gross features of the jet.

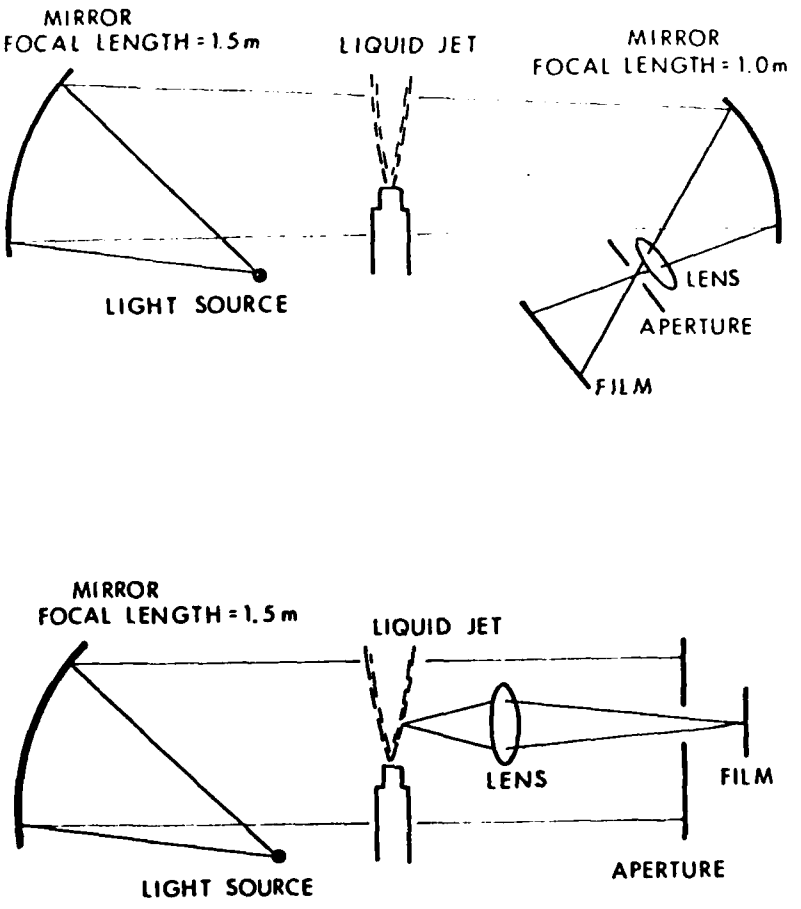

Figure 2 . Photographic Methods Used for Studying the Jet and Droplets

E. Single Flash Set-up

The optical set-up was changed to the arrangement shown in the lower half of Figure 2 in order to examine the jet in greater detail. The light source was replaced with a single spark system* with a duration less than one microsec. The duration proved to be adequate for the tests. In addition, an f-3 lens was inserted into the system giving a magnification of about three (Figure 2). Ultimate resolution, based on the Rayleigh criterion, was about 3 μm, although this was not realized due to diffraction problems.

A Graflex camera, without the lens, was employed and the event was recorded on Kodak Royal-X Pan Film 4166 using the 4 x 5 in. film size. Enlarged prints of the negatives were made resulting in an overall magnification of about ten.

Several photographs were taken using various wire sizes for calibration purposes in order to examine the diffraction problem; namely, diameters of 13 μm, 25 μm, 76 μm and 254 μm. The spark system was the light source. Photographs were taken (a) with the wires in the approximate focal plane and (b) about 20 mm from the focal plane. Clear reasonably well defined images were recorded for all cases with the wires at the focal plane. At twenty millimeters from the focal plane the wire boundaries were not as sharp, resulting in more uncertainty in the width of the recorded image. Also, the diffraction pattern for the wires outside the focal plane resulted in increased width of the diffraction lines as expected based on the study of Fresnel diffraction patterns by De Corso[40]. Table IV illustrates the severity of the problem. The values in the Table were determined by inspection of the photographs using a simple eyepiece with a 0.1 mm scale.

The size of the images recorded on the film were as much as six times larger than the actual size for the 13 μm wire diameter. The uncertainty in wire size becomes less with increasing wire diameter, however, even for the 254 μm diameter wire, the apparent size is still about 20 % too large. The uncertainty with the larger wire sizes is due to the difficulty in selecting the actual edge of the wire boundary due to the lack of a sharp transition. Fresnel diffraction theory[41] gives a value of 0.25 for the intensity, relative to the maximum intensity, at the geometric edge. For the numbers summarized in Table IV, the edge that was selected was located at the first indication of a transition between a light and dark region.

*Courtesy of D. Shear, BRL. Spark system consisted of six 0.02 μF capacitors giving a total energy of 0.5 J when operated at 3 kV. Electrode separation was approximately 3 mm.

The uncertainty with the smaller wire sizes is due to the increased uncertainty in the transition region. It should also be noted that the center of the recorded images for the smaller wire sizes was not as dark as the center of the larger wire sizes.

Table IV Wire Diameter, Based on Readings of Photographs Using a Simple Magnifier

Actual Wire Size	At Focus		20 mm from Focus		At Focus	20 mm from Focus
	Apparent Wire Size Recorded on Film	Factor between Actual and Apparent Wire Size	Apparent Wire Size Recorded on Film	Factor between Actual and Apparent Wire Size	Size of First Bright Fringe	Size of First Bright Fringe
(μm)	(μm)		(μm)		(μm)	(μm)
13	77	5.9	170	13	29	52
25	81	3.2	176	7	34	52
76	114	1.5	150	2.0	36	72
254	310	1.2	398	1.6	52	77

With the exception of the wire sizes, all values have 10 - 30 % error with the larger errors associated with the smaller wires.

For the wires outside of the focal plane the diffraction problem was considerably worse. The apparent width of the wire was not only larger, but there was an increase in the width of the first bright fringe (function of wire diameter) and, also, more diffraction lines were produced.

Because of these problems, particles of about 100 μm were considered within the detectable range with an uncertainty in size of about ± 50 %. This conclusion seemed reasonable based on the photographs obtained by Seebaugh and Lee[27]. It was also apparent that droplets as small as 10 μm would be recorded on film, although determining their correct sizes would be highly speculative due to their unknown distance from the focal plane and the

problem of diffraction. The sizing problem can be solved, at least in principal, by performing a calibration of droplets of known size and of known distance from the focal plane as was done by De Corso[40] and then using a densitometer to integrate across the diffraction ring pattern as done by Menzel and Shofner[42] using the analysis of Born and Wolf[41]*. Such an undertaking goes well beyond the scope of the present study and was not further investigated.

F. Quantimat

The recorded wire images were also examined using a Quantimat Model 720 **. The Quantimat displays an image of the photograph on a screen. Since the boundaries of the wires displayed in the photographs are not sharp, it is possible to adjust the image of the wire to an arbitrary size depending on the brightness selected for the background screen intensity. By adjusting the background light intensity the Quantimat was calibrated using the image of the 13 μm wire. The image of the 25 μm wire was then examined. The value for the diameter indicated by the settings on the Quantimat was just twice the value the Quantimat indicated for the smaller wire. In other words, the Quantimat scaled exactly between the images of the 13 μm and the 25 μm wire. However, when the 76 μm wire was examined again using the same background intensity, the Quantimat indicated a value for the diameter which was only increased by 10 %. For the images of the wire sizes investigated, it was therefore concluded, that the distortion in the photographs due to diffraction was too great to evaluate any meaningful data.

---

* It should be pointed out that for the jet-droplet photos, the width of the first bright diffraction ring did not change very much. Instead, many drops showed a light center, similar to the out of focus wire photo. Also, many drops were recorded that were completely dark without any well defined diffraction ring.

** Courtesy of N. Klein, BRL.

G. Particle Sizing Interferometer

The particle sizing interferometer, described in Reference 43, consists of a probe volume formed by two interfering HeNe laser beams, a photo detector and a signal processor. The PSI offers a non-perturbing method for obtaining information on both droplet velocity and droplet size. Droplets traversing the fringes of the probe volume scatter light into a photomultiplier. The signal is then processed using a specially designed central processing unit built around a Z80 microcomputer.

The droplet velocity is obtained by dividing the effective fringe spacing by the reciprocal of the frequency of the scattered light signal. The effective fringe spacing is based on the spacing between the fringes formed by the interference between the light scattered from the droplet and the actual fringes of the probe volume.

The droplet size measurement is based on the recorded visibility function, defined as the ratio of the AC signal to the DC component. Two analyses are applicable depending on the droplet size range. These ranges are, for small particles, 0.3 μm to 6 μm, and, for large particles, 6 μm to several hundred μm. In both cases the recorded visibility function can be related to the droplet size using Mie theory [43] for the small droplets and the refraction theory of Bachalo[38,43] for the large droplets.

Additional information on the droplet concentration is also estimated by the processor. An estimate of the droplet concentration is determined from a statistical analysis of the total number of recorded events divided by a normalized probe volume which is based on the effective fringe spacing.

Various logic circuits are built into the processor and include (1) a periodicity test which automatically excludes aperiodic signals falling outside of arbitrarily preselected limits and (2) visibility signals with ratios of AC to DC components which specify the visibility range over which signals are accepted. The limits on the visibility function are set in the processor which automatically accepts or rejects the signal.

IV. PHOTOGRAPHIC RESULTS

A. Introduction

The first series of pictures taken were of the jet as it emerged from the nozzle. Both single spark exposures (Test Series 1*) and high speed photographs (Test Series 2-4) were taken using the set-up illustrated in the upper half of Figure 2. Later photographs (Test Series 7,9-12) were based on a spark system and an imaging lens as shown in the lower half of Figure 2. With this set-up it was possible to examine in greater detail the jet fragments, droplets and boundary region. For the photographic studies with the spark light source, only water and the fluid LP were used.

For the single shot spark illuminated photographs, the spark timing trigger was set to function after approximately one half of the fluid was ejected. Photos were taken with the field of view centered both near the nozzle and about 150 mm from the nozzle. When comparing the photographs, care should be taken to examine the same region from the jet center line. In the cases where the center core jet has broken-up, as with the low pressure injection tests, the location of the jet center is questionable. However, by taking into account the droplets in the vicinity of the transparent scale (each division equals one millimeter), it should be possible to estimate the center line of the jet where the larger droplets are concentrated.

The photographs were taken under conditions that roughly approximated the conditions listed in Table III that were selected for the analytical calculations. These conditions included an ejection velocity of 100 m/s from a 1.6 mm diameter nozzle. Additional experimental variations were made and included a variation in injection pressure from two different nozzles.

---

* In Tables 5 and 6, the number of the First Series is given by the first figure in the column under Test No.

B. Jet Photographs

Photographs of the jet were first taken over a large viewing field of about 150 mm in order to obtain general information on the characteristics of the jet. The optical set-up is illustrated in the upper half of Figure 2. Both high speed photography with a multi flash system (Section III-D) and a single spark system (Section III-E) were used.The photographs with the large viewing field were taken at injection pressures of 31 MPa and 62 MPa. The high speed photography, although not offering fine resolution due to the flash duration, was still adequate for estimating the jet velocity, distance to jet core breakup, total injection time, and for a few tests, both the jet core divergence and an outer spray divergence. Estimates of the jet velocity were made by measuring, in successive photographs, the location of the tip of the jet. The measured data on the jet core divergence is not considered as accurate as the data obtained later using the single spark system. A summary of the high speed photographic test conditions and results is given in Table V.

The high speed photographs also revealed a fine spray-like appearance radiating from the jet core, in some cases at rather large angles from the jet axis. Resolution on the films was not adequate to identify any possible structure on the spray. The spray angles varied between tests with most of the radiating sprays at angles between 30° to 40° from the jet axis, i.e. about ten times the divergence of the jet boundary.

In order to improve the detail of the photographs, the flash system was replaced with the single spark system which provided a shorter duration light pulse. A summary of the test conditions and results is given in Table VI. This table summarizes the tests with both the large field of view (Test Series 1) and with the magnified view (Test Series 7, 9-12). A Summary of the photographs with the large field of view will be given first. Two photographs of the jet are shown in Figures 3 and 4. For these photos a razor blade was inserted into the light path on the camera side of the event. Blocking the light in this manner provided a method for observing the jet boundary layer, due to the scattered light, as the jet emerged from the nozzle. Without the razor blade the contrast showing the outer boundary layer was not as apparent due to the bright background. Location of the nozzle in these photos can be approximated by extrapolating the jet boundary back to the 1.6 mm diameter nozzle. It is clear from the original photographs that a fine spray exists in a boundary layer in the dark region near the nozzle.

TABLE V. HIGH SPEED PHOTOGRAPHS

Test No.	Fluid	High Voltage	Injection Pressure	Total Injection Time	----- Jet Tip ----- Distance from Nozzle	Velocity	Divergence Jet Core	Distance to Jet Core Breakup
		kV	MPa	ms	mm	m/s	deg	[redacted] (± 20 %)
2-1	Water	o	31	20.2	22	52	4	120
					51	60		
					90	93		
					142	108		
3-1	Water	20.2	31	20.6	73	108	-	125
4-1	Water	0	31	21.5	55	90	5	140
					104	101		
					155	98		
4-2	Water	20.0	31	20.5	76	107	4.5	100
4-5	Water	30.6	31	20.5	65	90	4	100
					111	96		
2-6	Water	0	62	16.2	59	92	-	150
					113	117		
2-4	Hexane	0	31	18.5	37	66	-	120
					80	106		
					132	104		
4-7	Hexane	20.4	31	18.4	56	83	4	> 135
					108	111		
4-8	Hexane	0	31	18.1	56	90	4	> 135
					106	105		

TABLE V. HIGH SPEED PHOTOGRAPHS (Continued)

Test No.	Fluid	High Voltage kV	Injection Pressure M. ı	Total Injection Time ms	----- Jet Tip ----- Distance from Nozzle mm	Velocity m/s	Divergence Jet Core deg	Distance to Jet Core Breakup mm (± 20 %)
2-2	LP	0	31	21.4	29	47	-	135
					54	49		
					86	80		
					129	88		
2-3	LP	0	31	17.6	118	101	-	145
4-3	LP	20.2	31	22.3	35	85	4	130
					81	88		
4-4	LP	20.2	31	22.8	40	78	3	110
					63	81		
4-6	LP	0	31	21.6	59	103	5	> 135
2-5	LP	0	62	18.1	83	135	-	130
2-7	LP	0	62	17.6	65	91	-	140
					120	127		
2-8	LP	0	62	16.9	83	117	-	80
					140	105		
2-9	LP	0	62	-	57	60	-	-
					92	73		
					132	81		

- indicates no data recorded

TABLE VI. SINGLE SPARK EXPOSURE

Test No.	Fluid	Injection Pressure MPa	Nozzle mm	Injection Time ms	High Voltage kV	Jet Core Divergence deg
1-2	LP	31	1.6	27	0	5
1-3	LP	31	1.6	24	0	5.5
1-4	LP	31	1.6	~ 27	0	4.5
1-5	LP	31	1.6	-	0	4
1-6	Water	31	1.6	23	0	5
1-7	Water	31	1.6	25	0	4
7-1	Water	31	1.6	-	0	-
7-2	LP	31	1.6	-	0	-
7-6	Water	31	1.6	-	20.5	-
7-7	LP	31	1.6	-	0	-
9-2	Water	31	1.6	-	0	-
9-3	LP	31	1.6	-	26.1	-
9-4	LP	31	1.6	-	0	-
9-5	Water	31	.52	-	26.8	-
9-6	Water	31	.52	-	-	-
9-7	LP	31	.52	-	26.2	-
9-8	LP	31	.52	-	-	-
10-1	Water	6.2	1.6	-	0	-
10-2	Water	6.2	1.6	-	26.1	-

TABLE VI. SINGLE SPARK EXPOSURE (Continued)

Test No.	Fluid	Injection Pressure MPa	Nozzle mm	Injection Time ms	High Voltage kV	Jet Core Divergence deg
10-3	LP	6.2	1.6	-	26.4	-
10-4	LP	6.2	1.6	-	0	-
10-5	Water	6.2	.52	-	26.0	-
10-6	Water	6.2	.52	-	0	-
10-7	LP	6.2	.52	-	26.7	-
10-8	LP	6.2	.52	-	0	-
11-1	Water	3.1	.52	-	26.0	-
11-2	Water	3.1	.52	-	0	-
12-1	Water	6.2	1.6	-	-	-
12-2	LP	6.2	1.6	-	-	-
12-3	Water	3.1	1.6	-	-	-
12-4	LP	3.1	1.6	-	-	-

- indicates no data recorded

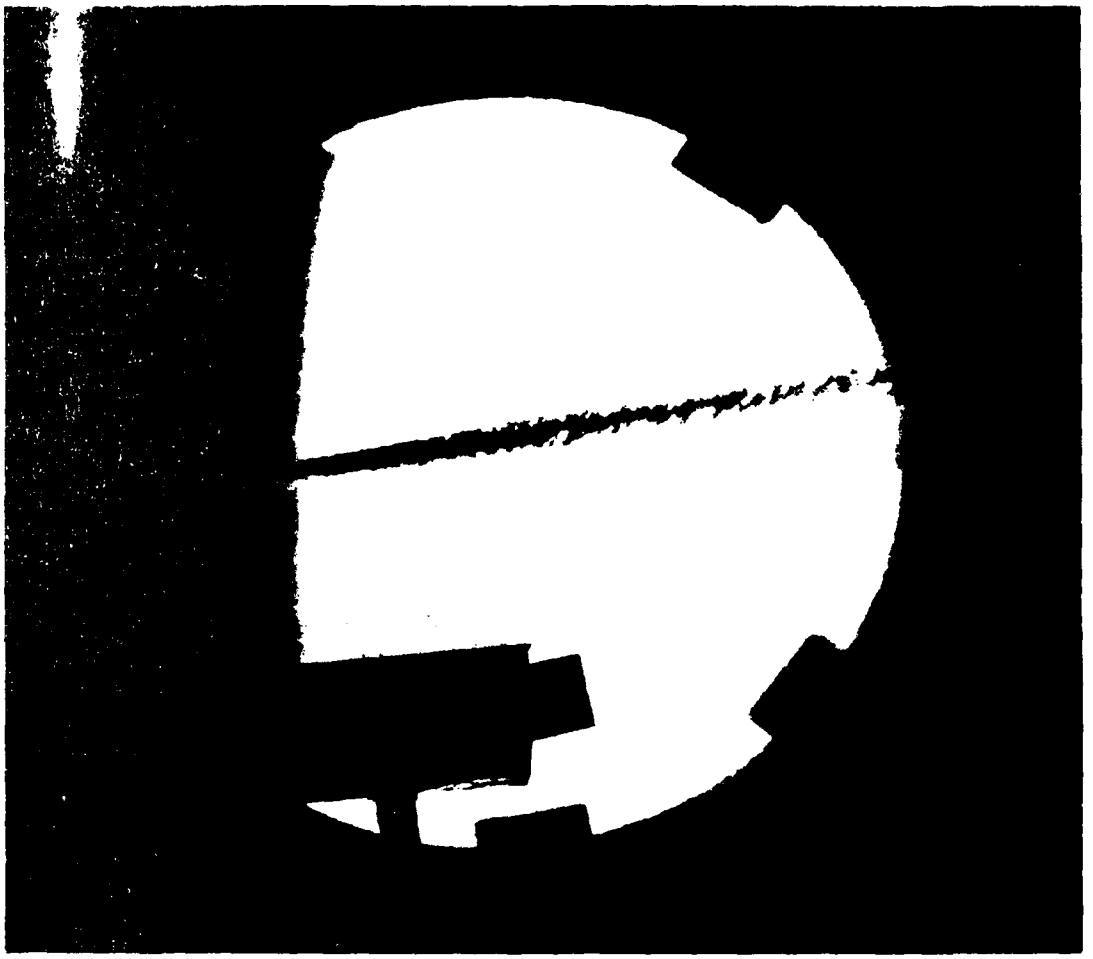

Figure 3. Jet of Fluid LP. Test Series 1-5

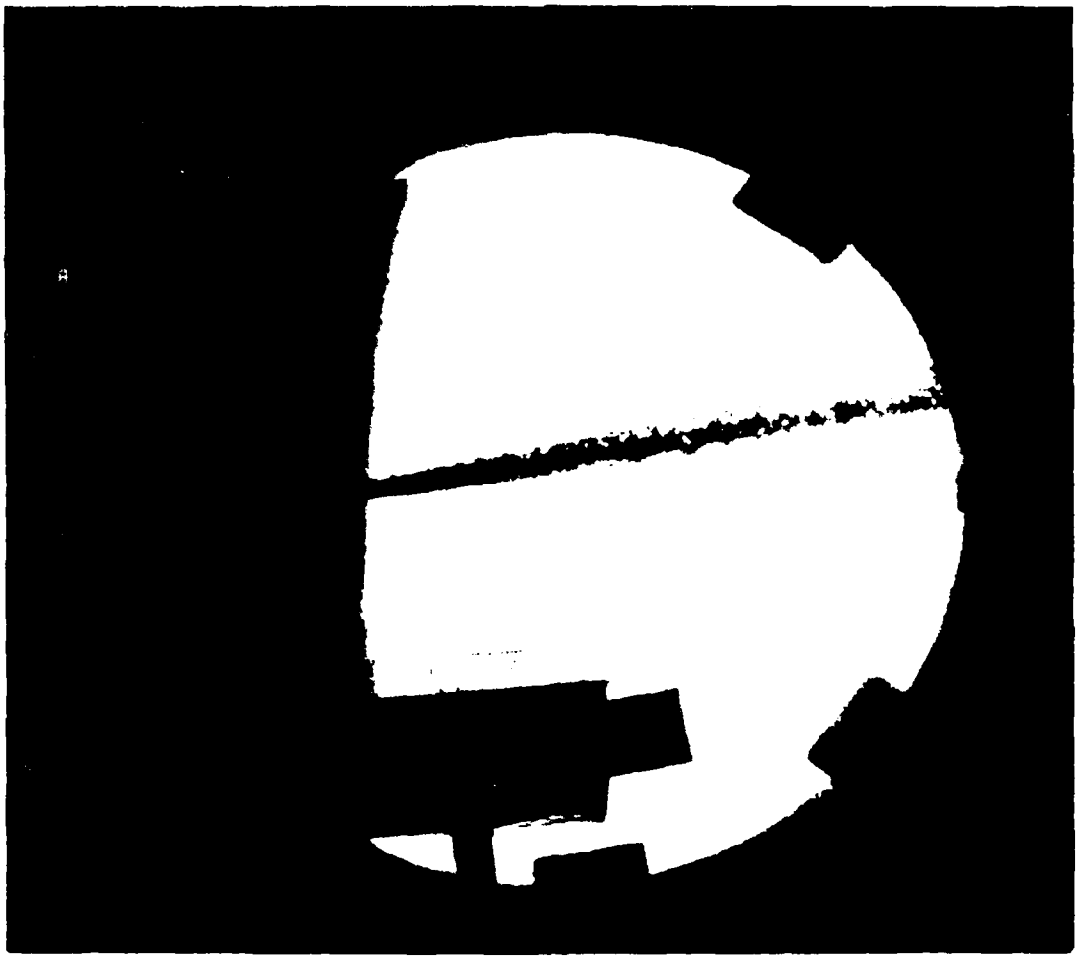

Figure 4. Jet of Water. Test Series 1-7

Figure 3, with fluid LP, shows a symmetric boundary layer while Figure 4, with water, shows considerable asymmetry in the boundary layer with the upper boundary emerging at an angle between 10° to 20° from the jet center core. This asymmetry in the outer boundary compares with the opaque jet boundary with a total divergence of about 4°.

The asymmetry in the jet boundary layer was observed in numerous cases. The nozzle was visually examined for possible defects or protuberances but none were detected. The cause of the boundary asymmetry may be associated with flow separation within the nozzle and the relatively low l/d ratio of the nozzle, foreign particles such as grease initially used to seal the fluid in the nozzle, or turbulent flow, a difficulty indicated by Lafrance and Ritter[9].

The outer boundary of the opaque center jet core for both water and the fluid LP remained linear over the first few centimeters until millimeter size disturbances began to distort the boundary. The disturbances frequently revealed a periodic structure, about 4 to 7 mm apart, which extended over several wave lengths. Extrapolating the early divergence of the center core showed a uniform total divergence (neglecting the initial boundary layer divergence) of 4 ° over the field of view. Other photographs showed similar features.

A summary of the jet data for the three fluids, based on the photographs over a relatively large field of view, is given in Table VII.

Table VII. Summary of Photographic Tests

Fluid	Injection Pressure	Orifice Diameter	Maximum Velocity	Discharge Coefficient	Jet Core Divergence	Distance to Jet Core Breakup
	MPa	mm	m/s		deg	mm
Water	31	1.6	105 ± 10	0.42 ± 0.04	4-5	100-140
Hexane	31	1.6	120 ± 15	0.39 ± 0.05	4	120- ?
LP	31	1.6	93 ± 5	0.44 ± 0.02	4-5.5	110-160
LP	62	1.6	125 ± 15	0.42 ± 0.05	-	80-140

The maximum velocity and the accuracy of the estimate is based on a plot of the individual data points for each test from Table V and by extrapolating by eye the overall trend of the data*. The discharge coefficient, C_d, is calculated from the Bernoulli flow equation

$$C_d = v\ (\rho/2\ P_i)^{1/2}. \qquad (7)$$

The summary of the jet core divergence data is taken from Table VI for water and the fluid LP and from Table V for Hexane. The summary of the estimate on the distance to where the jet core breaks up, is obtained from the data in both Tables V and VI.

C. Jet Emergence from Nozzle

In order to examine the jet as it emerged from the nozzle in greater detail, the optical set-up was changed to the system shown in the lower half of Figure 2. Figure 5 and 6 show the jet emerging from the nozzle (Figure 5) and close to the nozzle (Figure 6) using the fluid LP and water. These photos show the circular droplet diffraction patterns similar to those illustrated in Reference 21. The photos are typical of some of our early photos**. Little difference is noted between Figures 5 and 6, except perhaps the upper boundary in Figure 5 (fluid LP) which shows more droplet formation. The lower jet boundary, for both cases, shows an interesting ligament formation starting almost at the nozzle. The asymmetry in both photos is similar to the boundary layer asymmetry observed in Figure 4. A substantially larger angular divergence, however, is noted in the enlarged photos near the nozzle, especially with Figure 5. The outer boundary of the droplets define a maximum divergence from the center core of about 30° for fluid LP(Figure 5) and 23° for water (Figure 6). The maximum divergence in the outer boundary layer as recorded on the film is probably associated with the relative rotational position of the nozzle. No care was taken to insure that the nozzle was in the same angular position in the photographs.

---

* Test 2-9 with fluid LP at an injection pressure of 62 MPa was not included in the summary in Table 7. Test 2-9 indicated an abnormally low velocity, perhaps due to an incorrect pressure gage reading.

** Later photos, taken with more care in the optical set-up, especially with clearer optical surfaces; with the jet located at the focal plane, and with the proper film developer (which enhanced the final contrast), showed considerable improvement in picture quality.

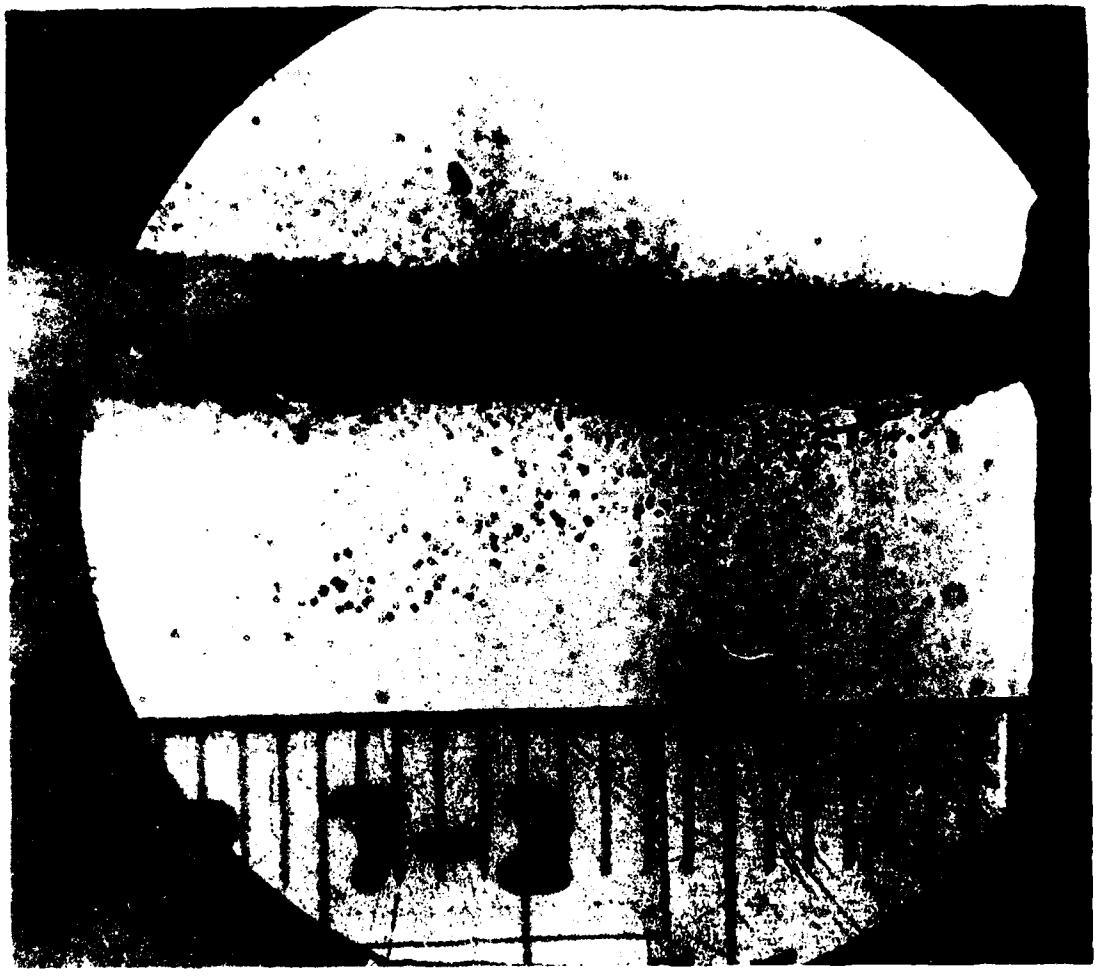

Figure 5. Jet of Fluid LP. Test Series 7-2

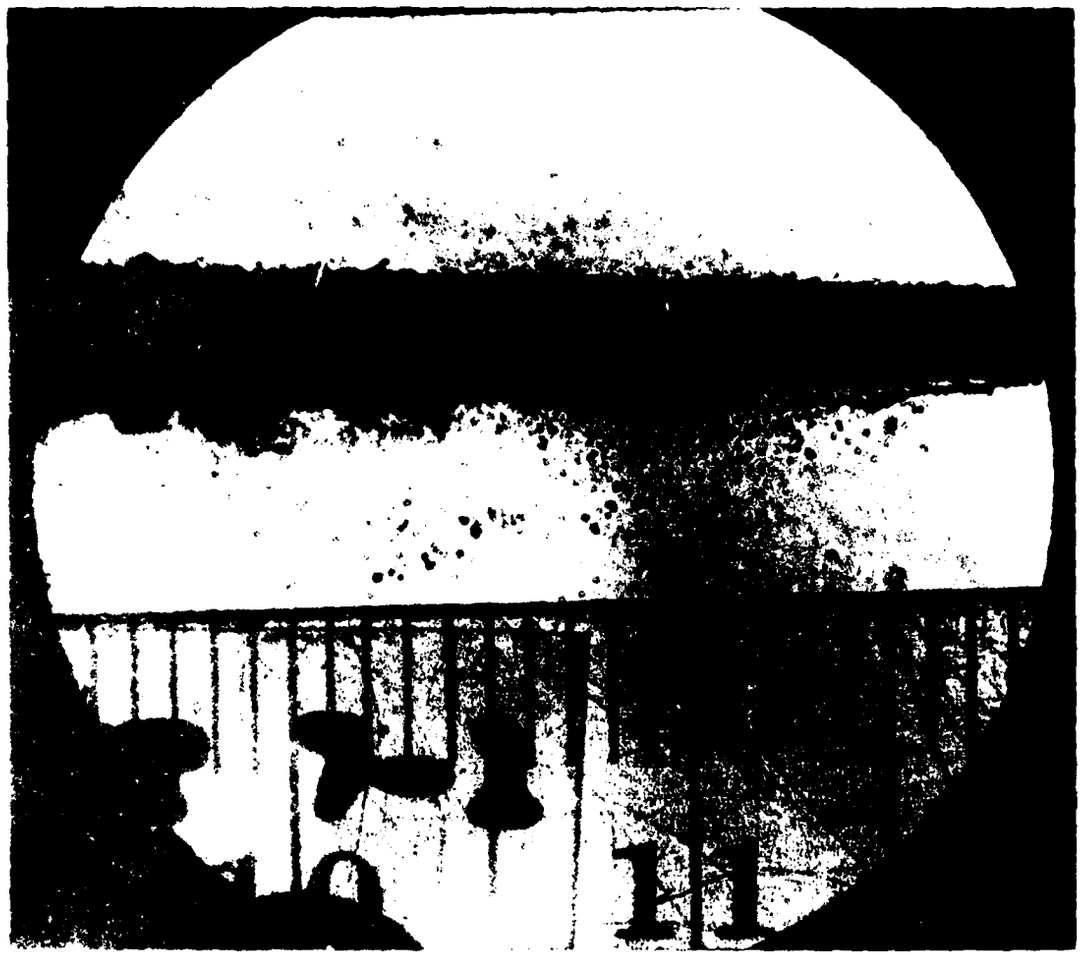

Figure 6. Jet of Water. Test Series 7-1

The total divergence of the opaque center core jet is 5° for fluid LP (Figure 5) and about 4.3° for water (Figure 6). The differences are probably not significant. The divergence in the field of view is essentially linear with a greater turbulence level noted on the lower jet boundary in both photos.

D. Effect of Injection Pressure

From the Bernoulli flow equation and the exponential dependencies summarized in Table III, the effect of injection pressure on the droplet size should have a square root dependence. Thus, a variation in pressure over a factor of ten should change the droplet size by a factor of about three. Photographs of the water jet using the 1.6 mm nozzle were taken at 3.1 MPa, 6.2 MPa and 31 MPa and are shown in Figures 7-9. In Figure 7 with an injection pressure of 3.1 MPa, the smallest solid dark droplets are estimated to be about 50 μm with a first bright diffraction ring of between 15 μm to 20 μm in width. Numerous larger droplets are also present varying in size up to about 500 μm with a first bright diffraction ring width of about 50 μm. These measurements on the droplet size can only be considered an upper limit.

In Figure 8 with an injection pressure of 6.2 MPa, the droplet concentration has increased substantially. These first two figures are of interest as they show numerous large globules in various stages of breaking-up. The smallest completely dark droplets in Figure 8 are estimated to be about 40 μm.

In Figure 9 the injection pressure was increased to 31 MPa resulting in increased droplet shearing. Boundaries of the larger liquid fragments show droplets (especially under further magnification) in various stages of shear. Droplet images are not as sharp due to the higher jet velocity, although individual droplet diffraction patterns are still visible. The liquid fragments a few millimeters from the jet core are highly irregular compared with the more smooth and circular shapes of the globules observed at lower pressure.

Clearly, these photographs are not adequate for verifying the anticipated factor of three for the change in the droplet diameter between Figures 7 and 9.

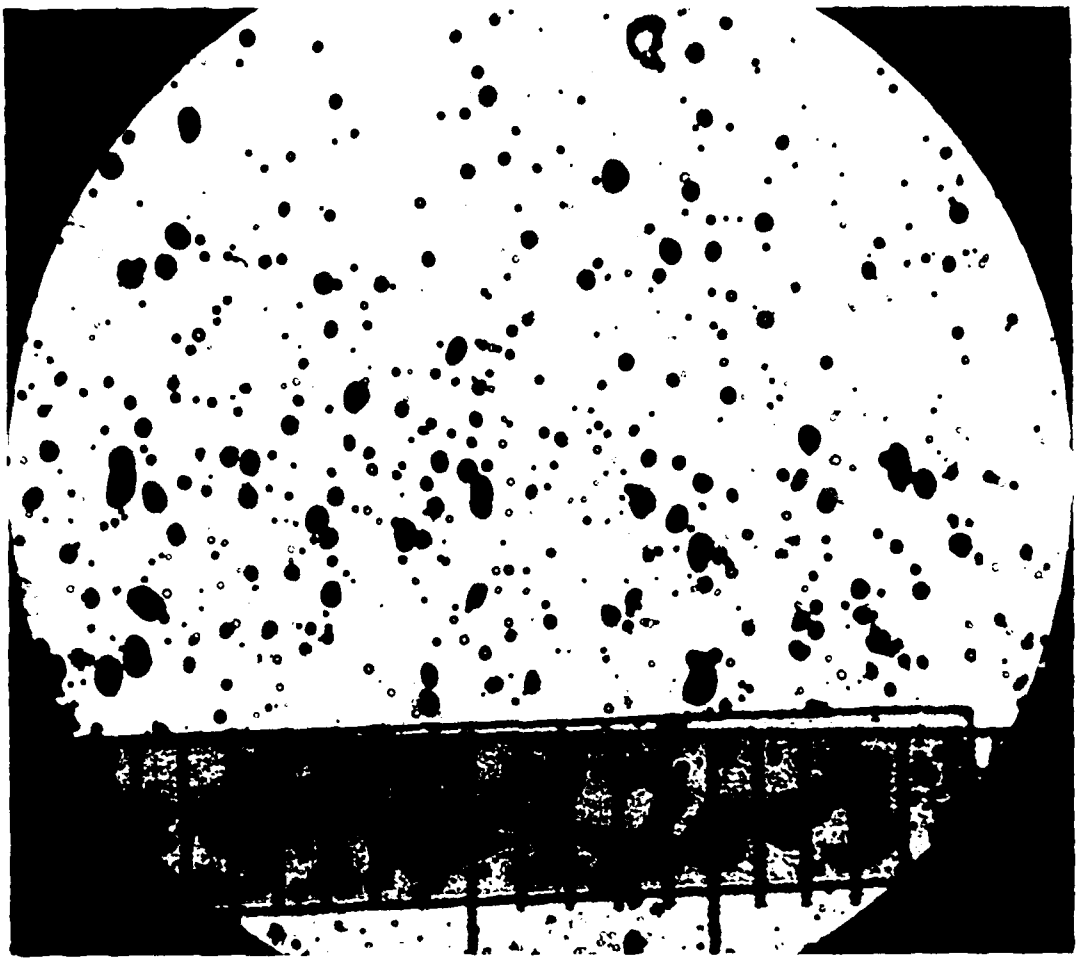

Figure 7. Jet of Water at an Injection Pressure of 3.1 MPa. Test Series 12-3

Figure 8. Jet of Water at an Injection Pressure of 6.2 MPa. Test Series VJ-1

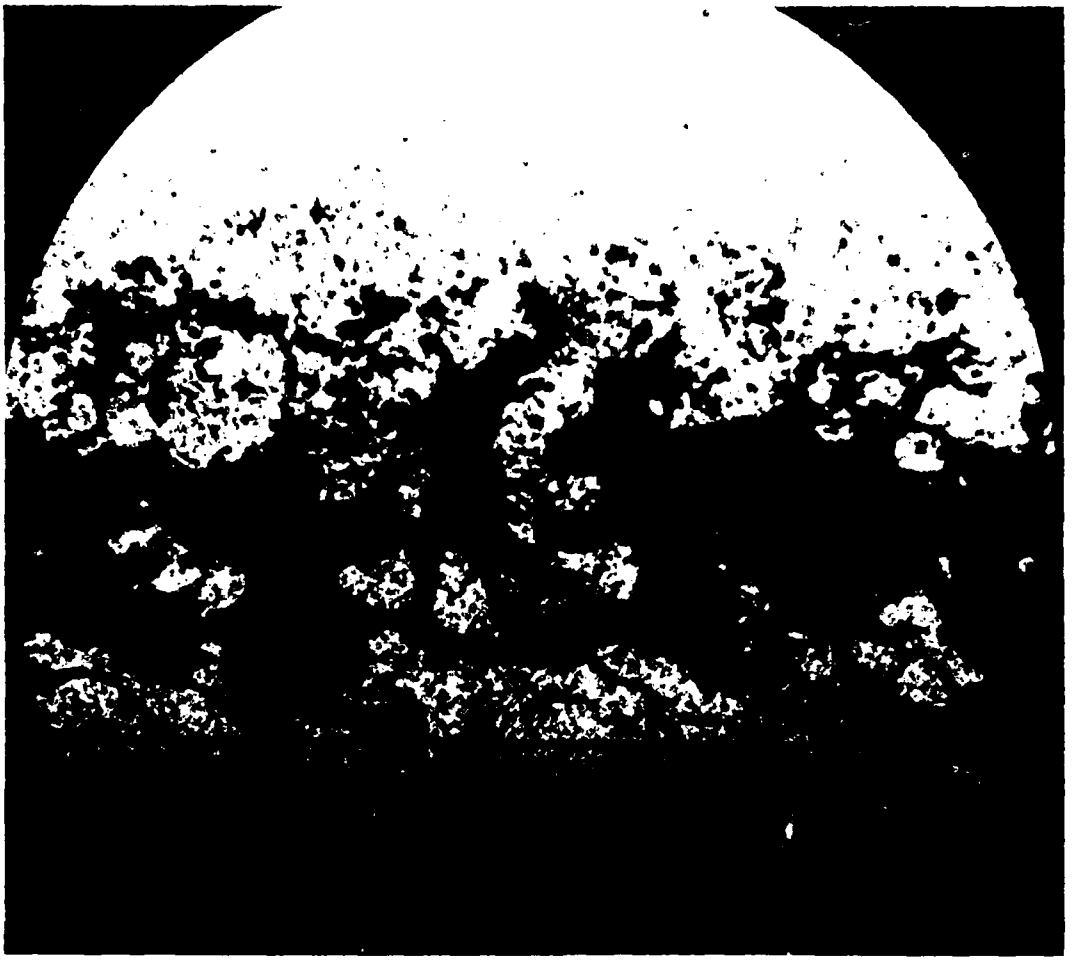

Figure 9. Jet of Water at an Injection Pressure Of 31 MPa. Test Series 9-2

E. Effect of Fluid

Photos were also taken with fluid LP at the 3.1 MPa, 6.2 MPa and 31 MPa injection pressures and are shown in Figures 10-12. The photographs at the two lower injection pressures show the same general features as the corresponding test with water, Figures 7 and 8. Figure 10 gives the appearance of a larger droplet concentration than Figure 7, however, the difference in apparent concentration is likely due to the location of the center of the jet closer to the center of the photo in Figure 10 and closer to the scale in Figure 7. Figure 12, at an injection pressure of 31 MPa, shows the same general features observed for the water injection tests. The jet breakup produces highly irregular fragments that are in the process of disintegrating further due to boundary shear. As with Figure 9, an examination of the surface of the fragments shows a rough surface in the process of droplet shearing.

No single spark exposures were taken using Hexane, however, several high speed photographic tests were made. The tests with Hexane, at an injection pressure of 31 MPa, indicated a much finer spray when compared with either the water or the liquid monopropellant jets. No significant differences were noted between water and the liquid monopropellant spray from the high speed photographic tests.

F. Effect of Nozzle

Figures 13-15 show a jet of water when ejected from the small nozzle (diameter = 0.52 mm, l/d = 17) at pressures of 3.1 MPa, 6.2 MPa and 31 MPa. When compared with the photos from the larger nozzle (diameter = 1.6 mm, l/d = 4.0) and at the same injection pressures, Figures 7-9, it is readily apparent that the resulting droplets are considerably smaller; the jet is broken into smaller globules, and the droplets probably fall into a narrower size distribution. Figure 13, as with Figure 7, illustrates relatively smooth globules in various stages of breaking-up. Figure 14 suggests that the globules may be more iregular when compared with Figure 8, however, in Figure 8 the center of the jet is located in the vicinity of the scale whereas in Figure 14 the remains of the jet is closer to the center of the photo. Figure 15 indicates a fine droplet spray without the large iregular shaped fragments which dominate the jet from the larger nozzle.

Possible differences in the jet and droplet patterns between water and liquid monopropellant are not readily apparent. For example, Figure 16 with liquid monopropellant ejected at 31 MPa, shows similar patterns when compared with the water jet in Figure 15.

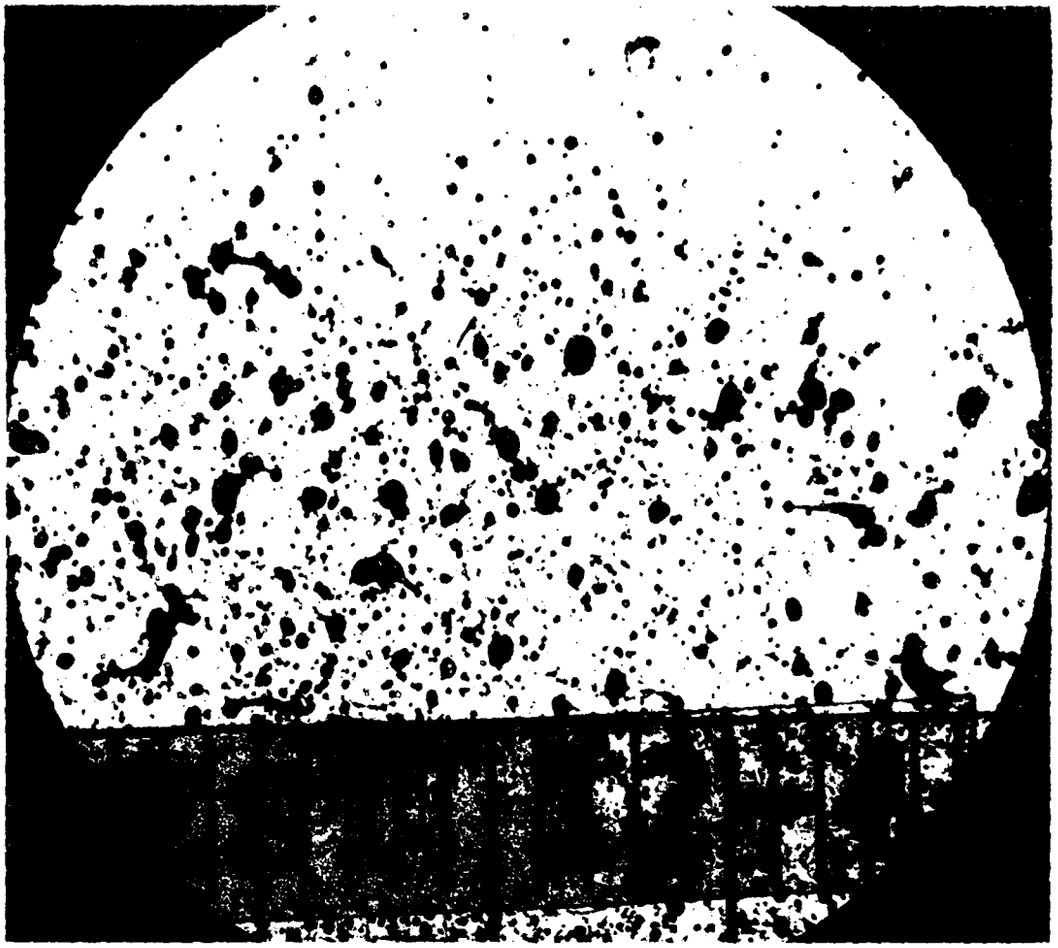

Figure 10. Jet of Fluid LP at an Injection Pressure of 3.1 MPa. Test Section 1-1

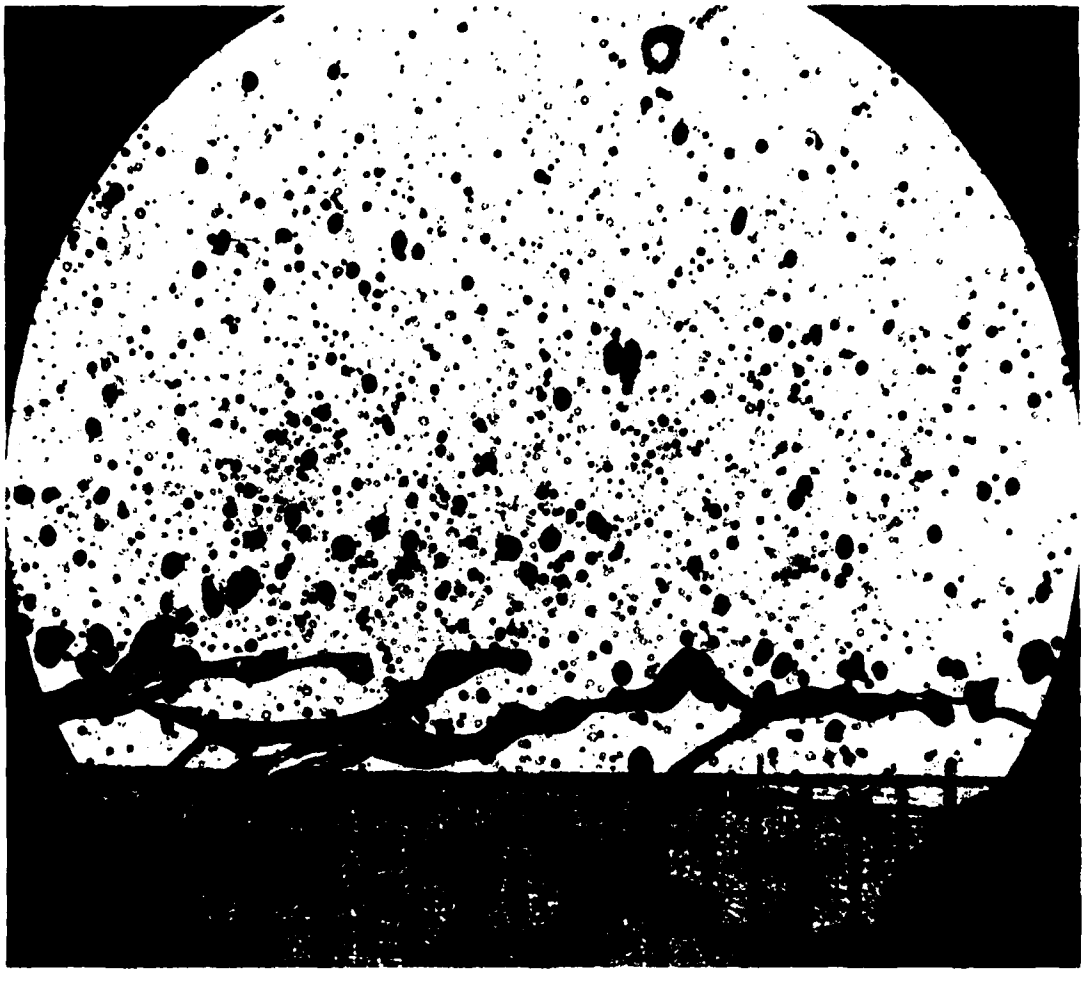

Figure 11. Jet of Fluid LP at an Injection Pressure of 6.2 MPa. Test Series 12-2

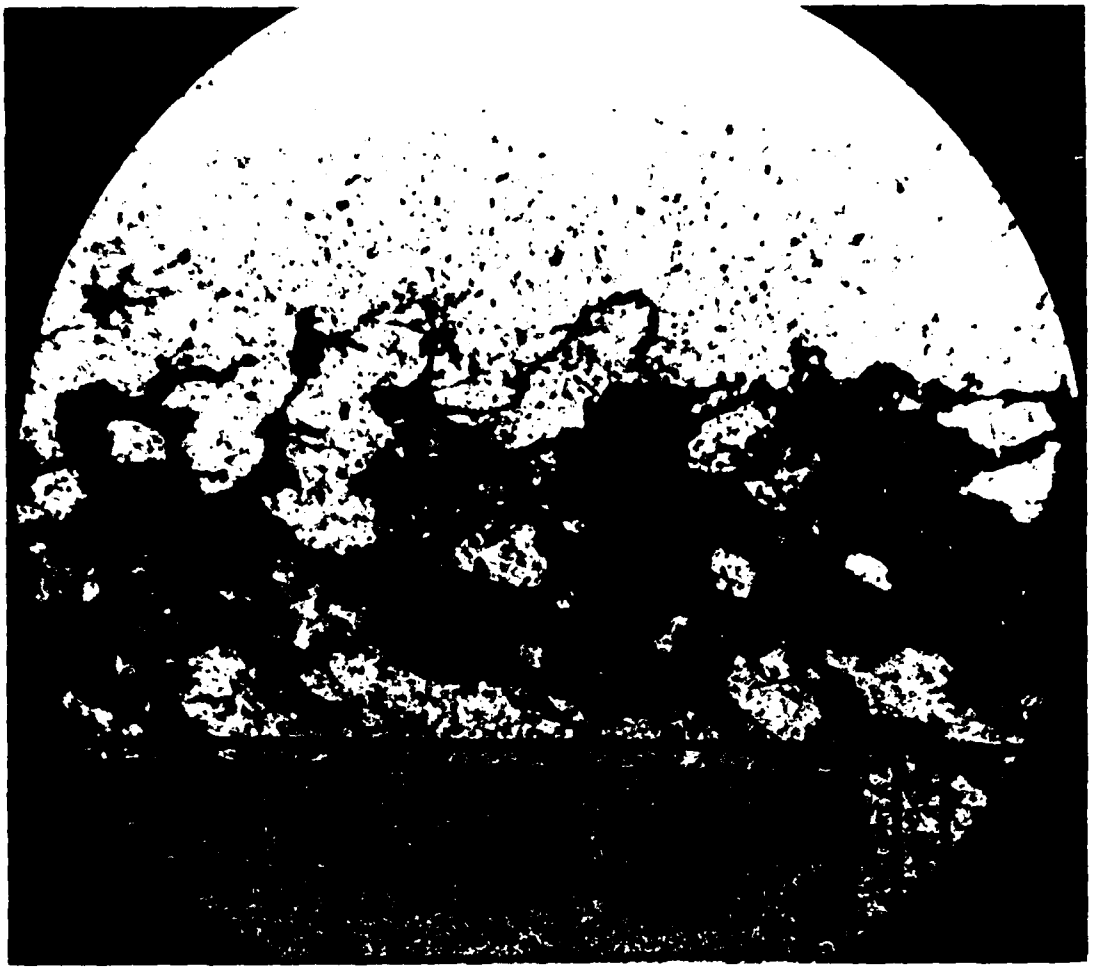

Figure 12. Jet of Fluid LP at an Injection Pressure of 31 MPa. Test Series 9-4

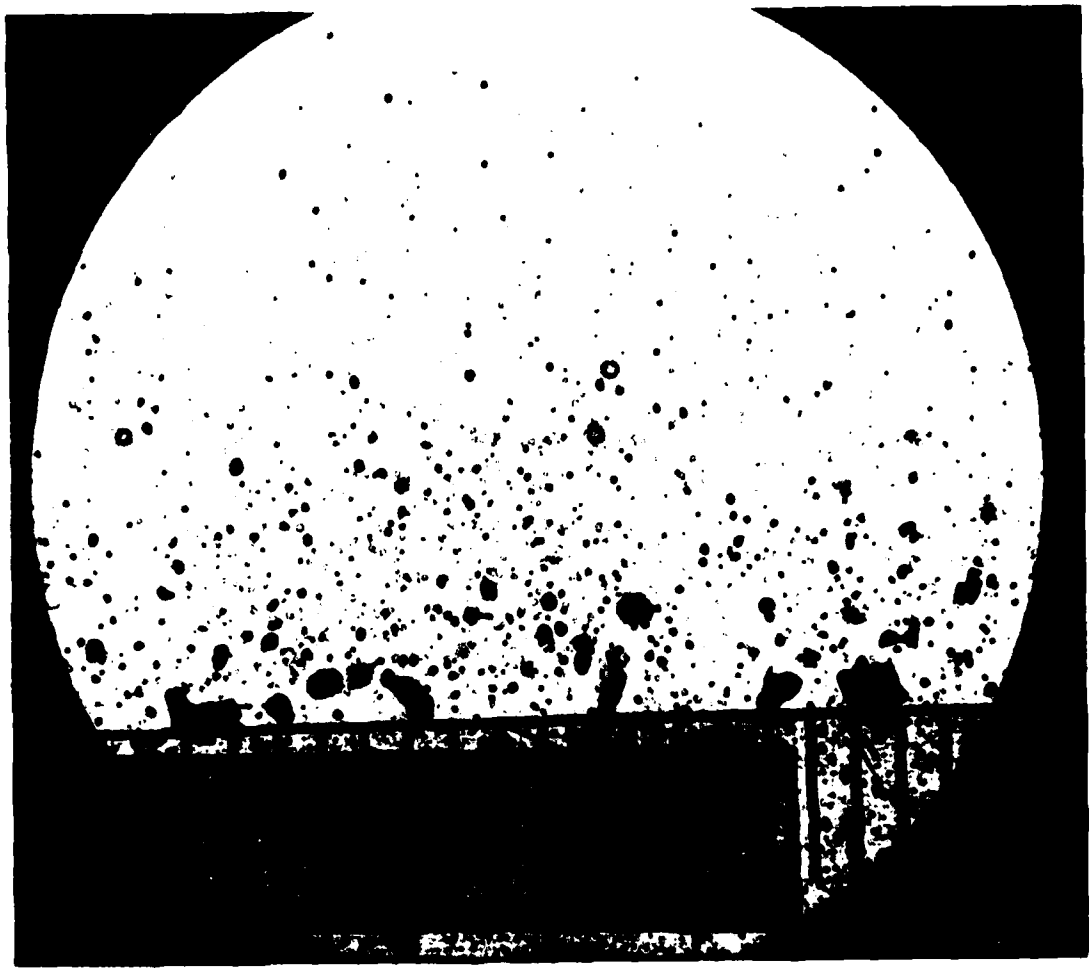

Figure 13. Jet of Water at an Injection Pressure of 3.1 MPa and with a Nozzle Diameter of 0.52 mm. Test Series 11-2

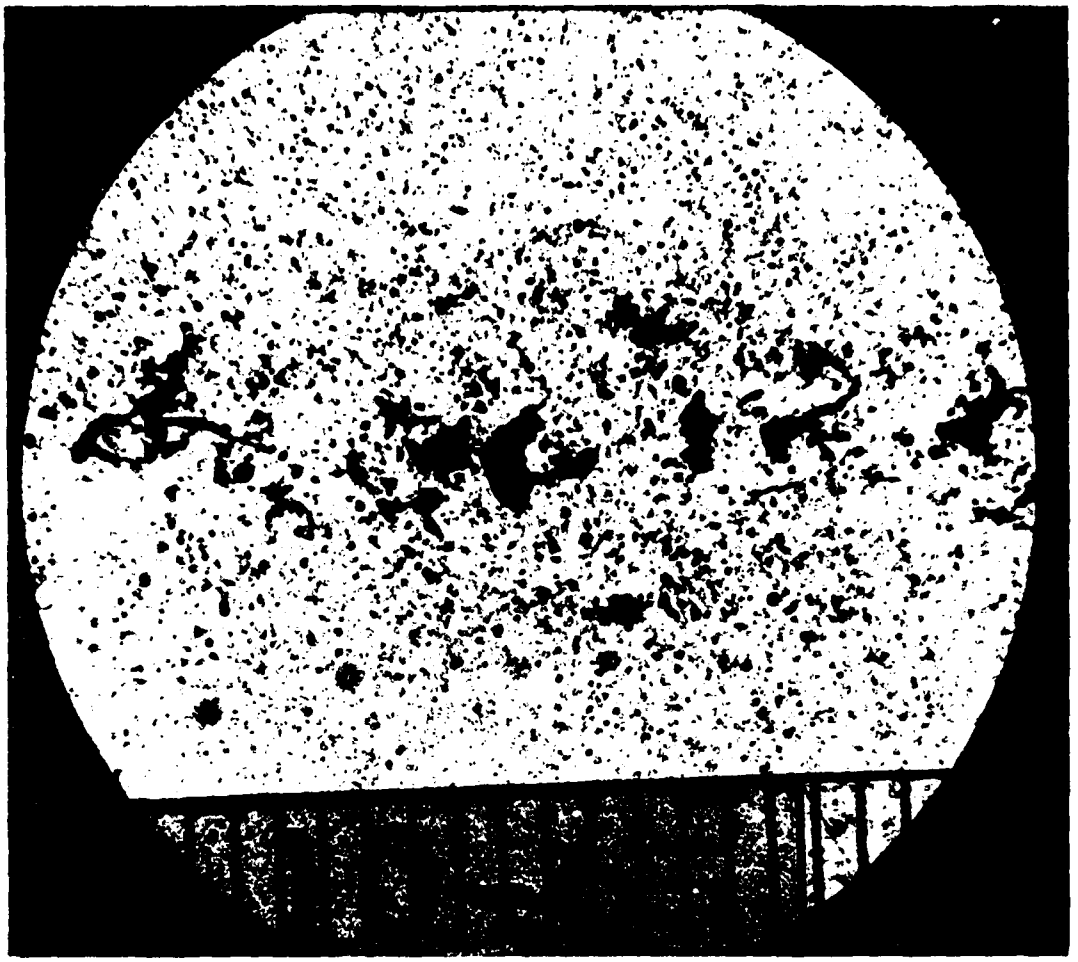

Figure 14. Jet of Water at an Injection Pressure of 6.2 MPa and with a Nozzle Diameter of 0.52 mm. Test Series 10-6

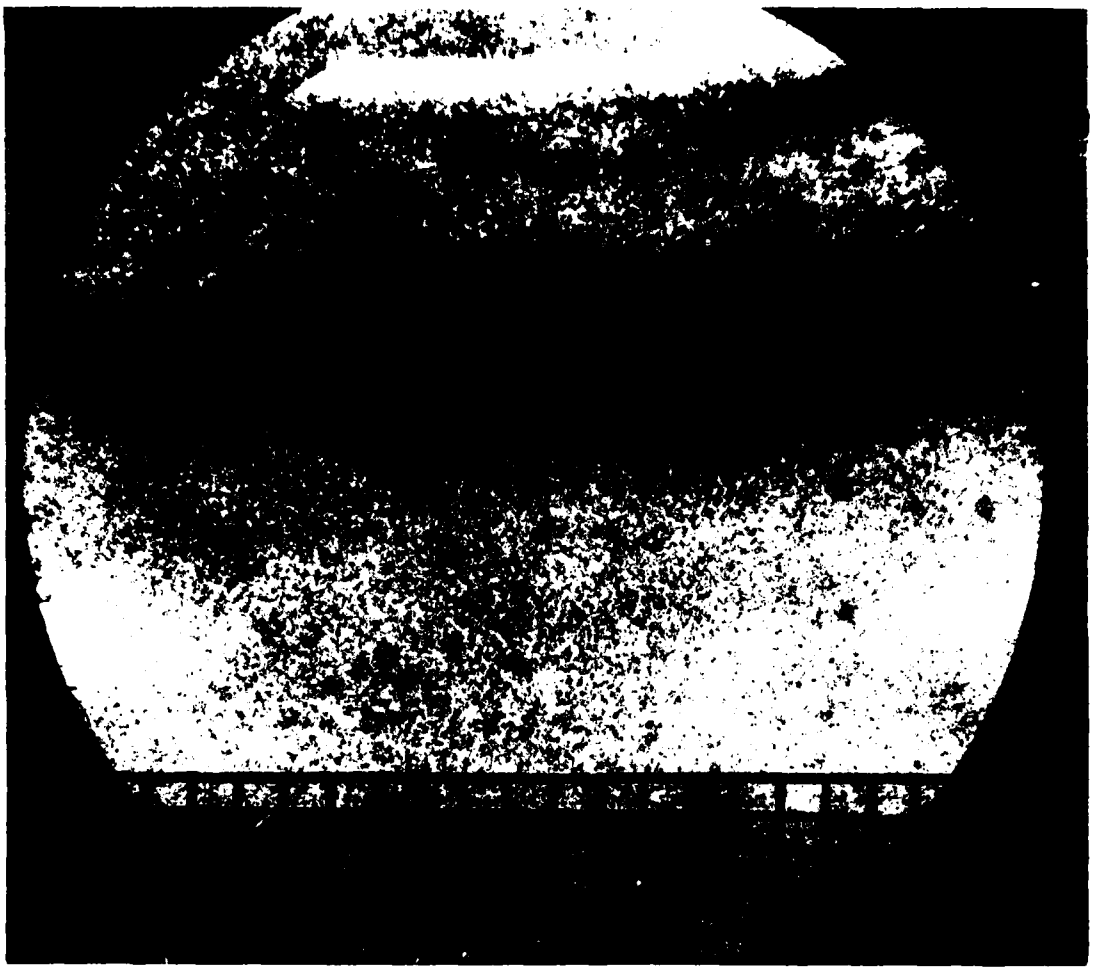

Figure 15. Jet of Water at an Injection Pressure of 31 MPa and with a Nozzle Diameter of 0.52 mm. Test Series 9-6

Figure 16. Jet of Fluid LP at an Injection Pressure of 31 MPa and with a Nozzle Diameter of 0.52 mm. Test Series 9-8

G. Effect of High Voltage

Figures 17 and 18 show a water jet after being ejected through an electric field at injection pressures of 3.1 MPa and 6.2 MPa. These photos were taken with the small nozzle. In Figure 17 both electrode plates were + 26 kV relative to the nozzle and in Figure 18 only one electrode plate was at + 26 kV relative to the other electrode plate and the nozzle. These photos may be compared,respectively,with the jets ejected under similar conditions, but with no electric field, which were shown in Figures 13 and 14. Based on the studies by Weinberg[44] and others, such as Savage and Hieftje[45] , on the effect of electric fields on jets, we anticipated a finer dispersion of droplets with the electric field. A comparison of the two groups of photos, however, suggests just the opposite. That is, there appears to be not only fewer drops but also a wider size distribution for the two cases with the electric field.

The same trend is also noted for the liquid monopropellant(LP). Figures 19 and 20 are taken without and with an applied electric field. Both photos were taken using the large nozzle. The boundary region above the jet core suggests a larger concentration of droplets in Figure 19, the case without the applied field.

These observations with the electric field do not necessarily contradict the earlier findings. The most likely explanation is that finer droplets are produced by electrostatic forces but that they are removed from the field of view.Photographs with and without the electric field when viewing the jet as it emerged from the nozzle might help to clarify the uncertainty.

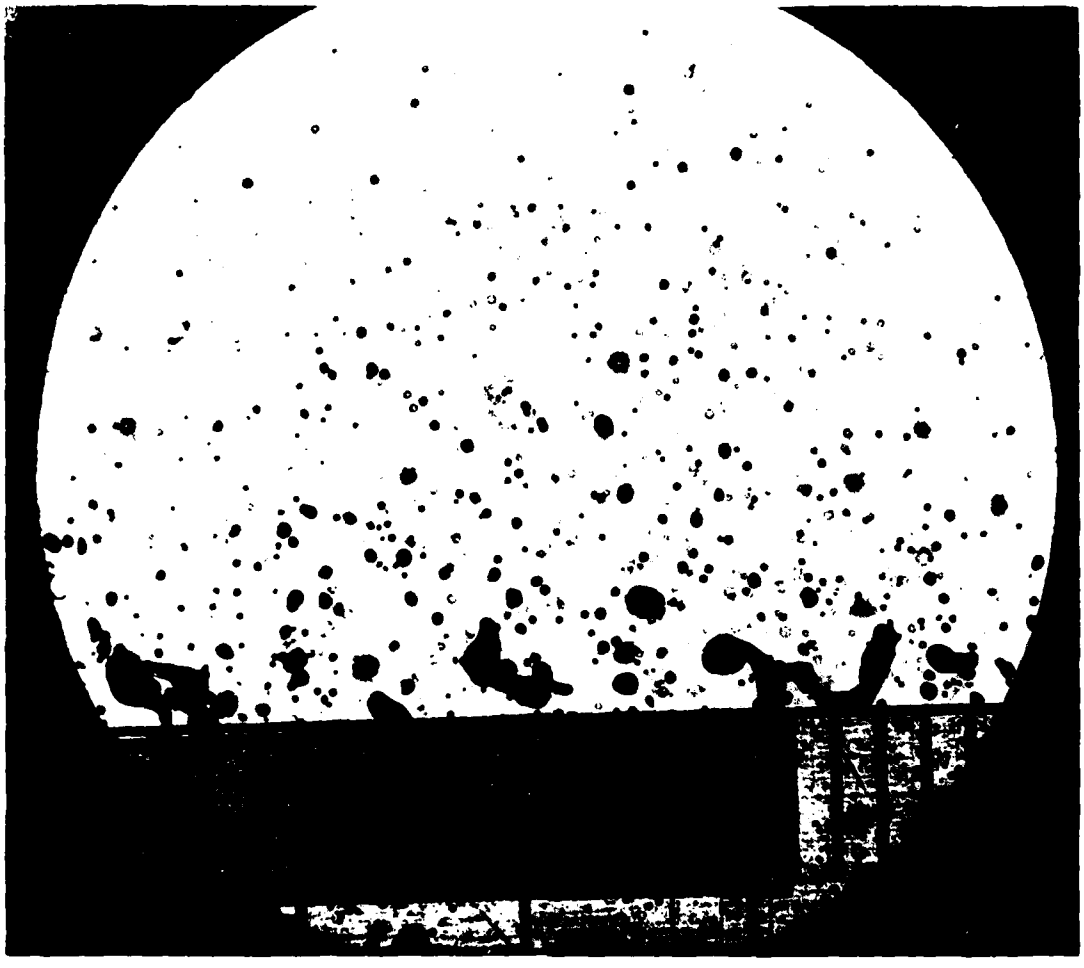

Figure 17. Jet of Water at an Injection Pressure of 3.1 MPa and with an Electrode Voltage of 26 kV. Test Series 11-1

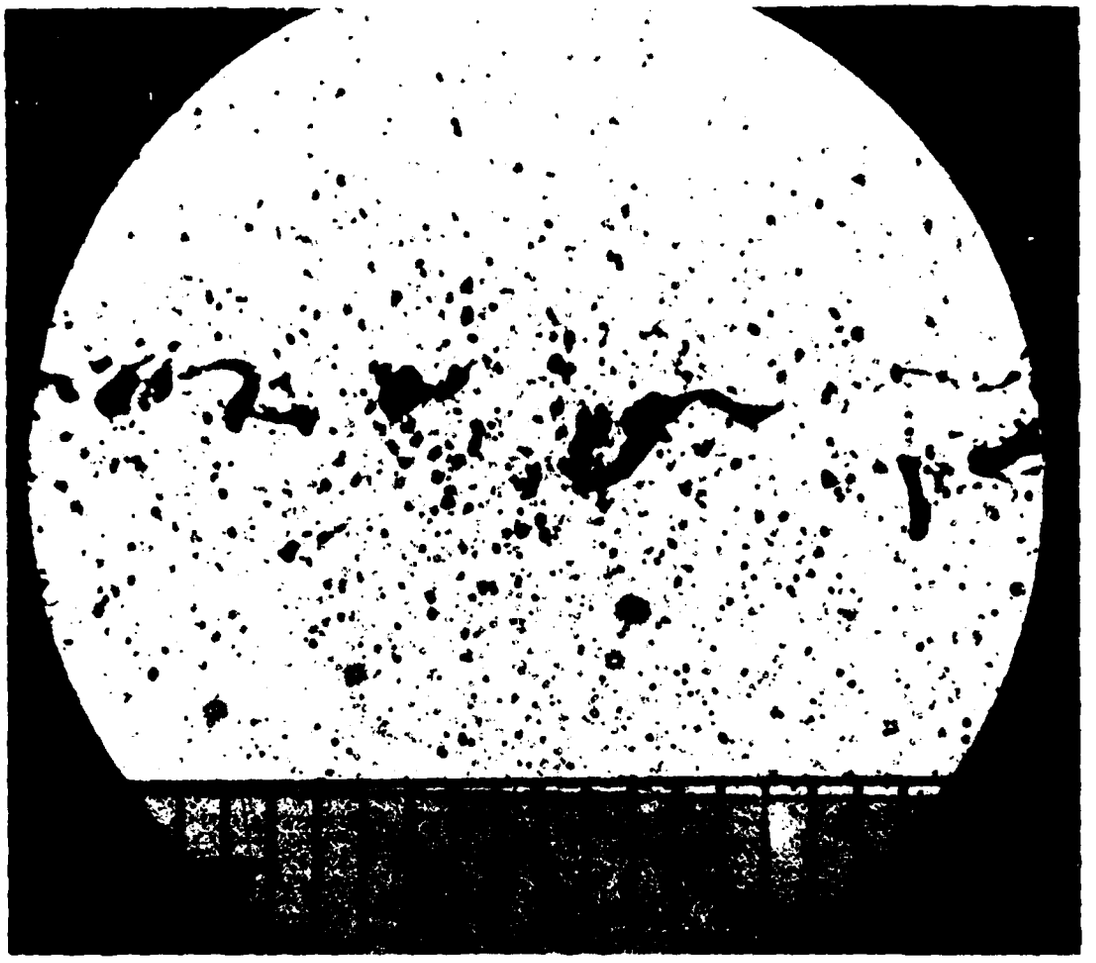

Figure 18. Jet of Water at an Injection Pressure of 6.2 MPa and with an Electrode Voltage of 26 kV. Test Series 10-5

Figure 19. Jet of Fluid LP at an Injection Pressure of 6.2 MPa and with Zero Electrode Voltage. Test Series 10-4

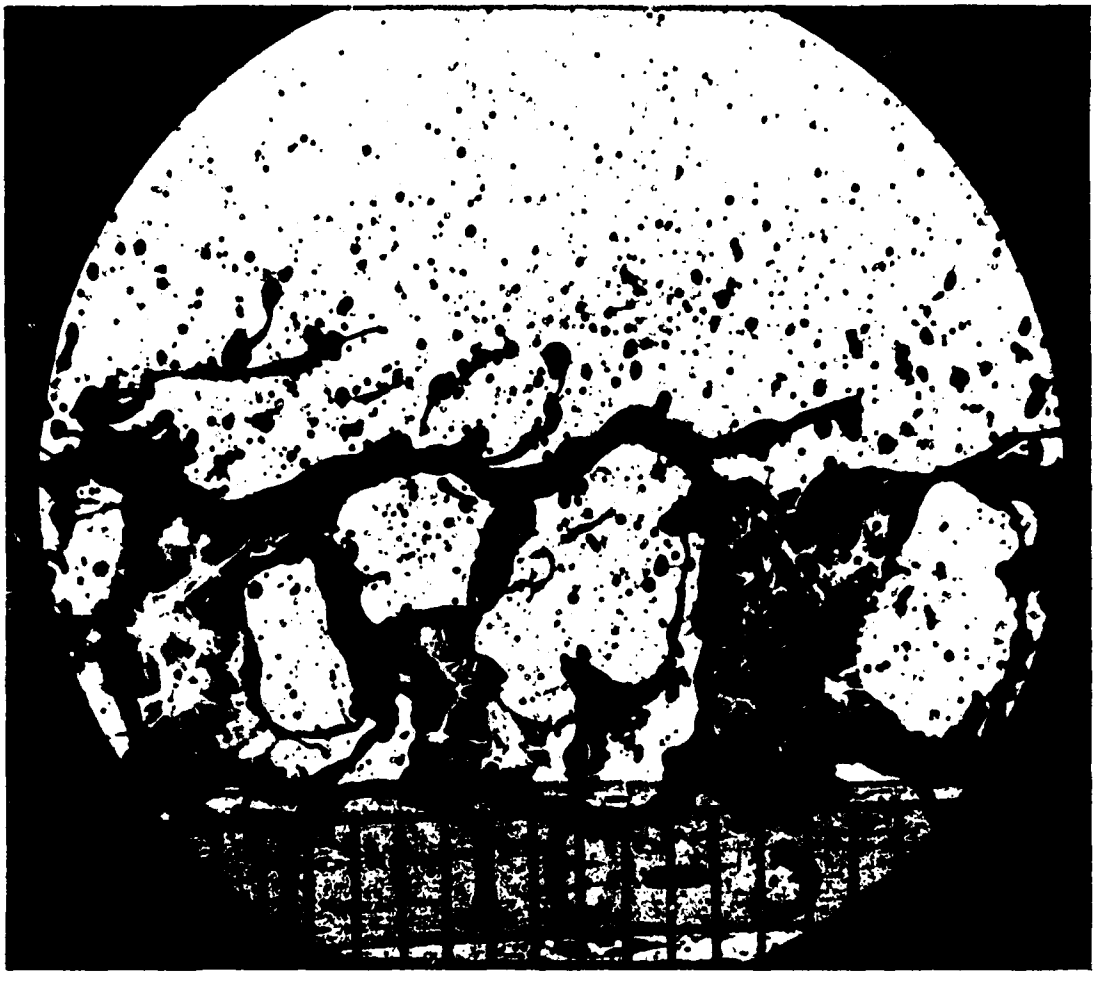

Figure 20. Jet of Fluid LP at an Injection Pressure of 6.2 MPa and with an Electrode Voltage of 26.4 kV. Test Series 10-3

V. RESULTS ON RELATED STUDIES

A. Particle Sizing Interferometer

Based on the photographic evidence and the characteristics of the particle sizing interferometer, it was not considered likely that any useful droplet velocity data would be obtained in the center core region of the jet because of the high opacity of the jets. Droplet data, however, from the boundary region was considered a possibility and attempts to make such measurements were tried at the BRL. These attempts were not successful. The difficulties were believed to be due to signal saturation problems resulting in an erroneous Doppler frequency (AC component of the visibility function). Attempts to correct this problem are now underway.

Some preliminary droplet and velocity data were obtained at the University of Tennessee Space Institute using water and a nozzle with similar characteristics as the 1.6 mm injection nozzle used at the BRL. A description of the tests and the results is given in Appendix B.

B. Propellant Ignition due to Frictional Heating

One concern during the study was whether ignition might occur during ejection of a monopropellant through one of the nozzles. A moderately energetic monopropellant was tested using both the 1.6 mm diameter orifice (l/d = 4.0) and the 0.52 mm diameter orifice (l/d = 17). Ignition was considered unlikely due to the high heat losses, however, the question of whether the frictional or shear heating was sufficent to produce ignition was considered important enough to warrant special attention.

The decision whether ignition occurred was based on both the photographic evidence and the subjective evidence consisting of an examination of the ambient atmosphere and an inspection of absorbent tissue which was impacted by the jet. For all tests no evidence of ignition was apparent.

VI. DISCUSSION AND CONCLUSIONS

No accurate droplet sizing data were obtained during the study. The photographs provided, however, an evaluation of the overall characteristics of the jet and, in addition, a semiquantitative estimate of droplet sizes with accuracies limited to about 100 μm for the droplets diameter. Smaller droplets were readily detected, down to at least 10 μm, but there was considerable uncertainty in actual sizes. No sizing data representative of the jets under study were obtained with the particle sizing interferometer. The data (Appendix B) that were obtained with the particle sizing interferometer suggested, based on the mean values of several tests, a plausible weak dependence between droplet size and velocity, a finding not unexpected due to the likely quasi-equilibrium conditions of the spray (either 43 cm or 89 cm distance between the nozzle and the probe volume). An examination of the individual data points for an individual test, however, did not support the possible droplet size vs.velocity dependence and no firm conclusions on the existence of a dependence between droplet size and velocity for an individual test can be given. The recorded mean droplet sizes varied between 52 μm to 64 μm and corresponding mean velocities varied from 7 m/s to 12 m/s.

Based on the photographs, the general features of the jets for the three test fluids at the higher velocities revealed a highly turbulent boundary region along the jet core with an average jet diameter that increased linearily with distance. Away from the jet core there was evidence of small drops that apparently were formed due to liquid shearing either first into ligaments which then broke up or directly into the small drops.

The agreement between the predicted jet breakup length and the observed breakup length was rather poor if the data are compared with the high velocity jet analysis of Levich[12]. For example, observed breakup lengths (Table VII)for the high velocity jet, which is assumed to be turbulent, exceeded the predicted values by factors of five to six. However, if the low velocity analysis of Weber[12] is used, then a more reasonable agreement is obtained between the observed jet breakup length and the predicted value.Clearly, therefore, the appearance of a turbulent jet may not warrant the assumption that the jet falls into a high velocity region dominated by a breakup process as described by Levich.

Various mean droplet correlations were examined (Table III); their accuracy can only be judged qualitatively due to the limitations noted previously on the estimates of the droplet sizes. It was apparent, however, that the droplet sizes in the photographs are considerably smaller than the values predicted by the various correlations. Also, the mean droplet sizes

indicated by the particle sizing interferometer (for the case where $v \sim 10$ m/s) were as much as 6 to 28 times smaller than the values indicated by the correlations. The theoretical correlation of Mayer[20] gave the smallest values for the droplet sizes, but was still a factor of six larger than the values indicated by the particle sizing interferometer.

One source of difficulty with the particle sizing interferometer may be associated with our failure to scan a sufficently large droplet region. The photographs showed that only in the outer boundary region there existed a uniform droplet concentration with a likely narrow band size distribution. As the jet core is approached, much larger and irregular shaped fragments are encountered which are likely in various stages of breaking up. Thus, characterizing a jet while in the breakup region with a single mean droplet value is a simplification which is not justified unless the measurements are made at a sufficently large distance from the nozzle. It was for this reason that the droplet sizes recorded with the particle sizing interferometer were measured at the rather large distance of 43 and 89 cm.

Differences in the general appearance between the water and fluid LP jets were negligible. For the Hexane jet a considerable difference was noted with a much finer spray. Three of the numerical correlations that were examined also predicted smaller droplets for the Hexane jet.

An interesting feature observed on many of the photographs was a droplet shearing immediately as the jet emerged from the nozzle. Because of the uniform circular cross section of the nozzle, flow separation within the nozzle may have occurred which, it is postulated, would cause increased turbulence in the jet boundary sufficient to induce a droplet shearing. Supporting the possibility of flow separation within the nozzle were the rather low discharge coefficients (Table VII) which varied from 0.39 to 0.44.

The photographs taken during the tests with the electric field indicated the unexpected results that larger drops were present for the case with the electric field. This observation may simply be due to the removal of the smaller drops from the field of view.

Although flow conditions were not increased to the maximum specifications of the test equipment, there was still no evidence of ignition of the liquid monopropellant LP for flow velocities up to 125 m/s through a 1.6 mm orifice.

REFERENCES

1. A.A. Putnam, F. Benington, H. Einbinder, H.R. Hazard, J.D. Kettelle, jr., A. Levy, C.C. Miesse, J.M. Pilcher, R.E. Thomas, A.E. Weller and B.A. Landry, Injection and Combustion of Liquid Fuels, Wright Air Development Center TR 56-344 (Battelle Memorial Institute, Contract No. AF 33 (038) 13501, 1957

2. Victor G. Forsnes and Richard D. Ulrich, A Literature Review and Discussion of Liquid Particle Breakup in Gas Streams, Naval Weapons Center TP 4589, 1968

3. Ed. David T. Harrje and Frederick H. Reardon, Liquid Propellant Rocket Combustion Instability, National Aeronautics and Space Administration, SP - 194, 1972

4. A.R. Jones, A Review of Drop Size Measurement - The Application of Techniques to Dense Fuel Sprays, Proc. Energy Combustion Sci, Vol. 3, pp 225-234, 1977

5. G.M. Faeth, Current Status of Droplet and Liquid Combustion, Proc. Energy Combustion Sci, Vol. 3, pp 191-224, 1977

6. Ed., Dwight E. Gray, McGraw-Hill, American Institute of Physics Handbook, p 2-187, 2-188, 2-181, 4-30, 4-32, 1963

7. W.S. Janna, and J.E.A. John, Drop-Size Distributions of Newtonian Liquid Sprays Produced by Fan-Jet Pressure Nozzles, J. of Eng. for Industry - Trans. of the ASME, pp 171-177, 1979

8. R.P. Grant and S. Middleman, Newtonian Jet Stability, A.I.Ch.E. Journal, Vol. 12, pp 669-678, 1966

9. P. Lafrance and R.C. Ritter, Capillary Breakup of a Liquid Jet with a Random Initial Perturbation, J. of Applied Mechanics, Trans. of the ASME, Vol.44, pp 385-388, 1977

10. J.A. Newman and T.A. Brzustowski, Behaviour of Liquid Sprays at High Pressures, AIAA Paper No. 70-8, AIAA 8th Aerospace Sciences Meeting New York, New York, Jan. 1970

11. V.A. Borodin, Yu.F. Dityakin, L.A. Klyachko, V.I.Yagodkin, Atomization of Liquids,Foreign Technology Division WP-AFB, Ohio, FTD-MT-24-97-68, 1967

REFERENCES

12. E.J.Rice, Reference 3, pp 49-55

13. R.A. Mugele and H.D. Evans, Droplet Size Distribution in Sprays, Industrial and Engineering Chemistry, Vol 43, pp 1317-1324, 1951

14. J.F. Groeneweg, Reference 3, pp 55-59

15. A. Lekic, R. Bajramovic and J.D.Ford, Droplet Size Distribution: An Improved Method for Fitting Experimental Data, The Canadian Journal of Chemical Engineering, Vol 54, pp 399-402, 1976

16. H.C. Simmons, The Correlation of Drop-Size Distributions in Fuel Nozzle Sprays, Part I: The Drop-Size/Volume Fraction Distribution, pp 309-314 and Part II: The Drop-Size/Number Distribution, pp 315-319, J.Eng. for Power, Section A, Trans. of the ASME, 1977

17. H. Sato and T. Sakai, The Distribution Function of Disintegrated Droplets, Ind.Eng.Chem., Fundam., Vol 16, pp 475-480 1977

18. P.G. Burman and F. De Luca, Fuel Injection and Controls for Internal Combustion Engines, Simmons-Boardman Publishing Corp., New York, 1962

19. M.A.Weiss and C.H. Worsham, Atomization in High Velocity Airstreams, ARS Journal, pp 252-259, April 1959

20. E. Mayer, Theory of Liquid Atomization in High Velocity Gas Streams, ARS Journal, pp 1783-1785, Dec. 1961

21. H.G. Houghton, Spray Nozzles, in Chemical Engineers' Handbook, 3rd Edition, Edited by J.H. Perry, McGraw Hill, pp 1170-1175, 1950

22. B.J. Matthews, R.F. Wuerker and D.T. Harrje, Small Droplet Measuring Technique, TRW Systems, Technical Report AFRPL-TR-68-156, July 1968 .
(AF Contract FO 4611-67-C-0105)

REFERENCES

23. A. Zanker, Nomograph - Quick Route to Mean Drop Diameter, Manufacturing Chemist and Aerosol News, pp 47-49, Sept. 1975

24. N. Dombrowski and P.C. Hooper, The Effect of Ambient Density on Drop Formation in Sprays, Chemical Engineering Science, Vol 17, pp 291-305, 1962

25. H.E. Wolfe and W.H. Andersen, Kinetics,Mechanism, and Resultant Droplet Sizes of the Aerodynamic Breakup of Liquid Drops, Aerojet-General Corporation Report No. 0395-04 (18) SP (Contract No. DA-18 108-405 CML 829), 1964

26. J.D. Knapton and I.C. Stobie, The Application of Fuel Air Propellant for Use in Weapons (U), BRL Report 1654, 1973 (Confidential)

27. W.R. Seebaugh and D.H. Lee, An Optical Method for Observing Breakup and Vaporization of Liquid Jets, Princeton University Aeronautical Engineering Report No. 647 (NASA Grant NSG-99-60) June 1963

28. W.M. Farmer, Measurement of Particle Size, Number Density, and Velocity Using a Laser Interferometer, Applied Optics, Vol 11, pp 2603-2612, 1972

29. W.M. Farmer, Observation of Large Particles with a Laser Interferometer, Applied Optics, Vol 13, pp 610-622, 1974

30. W.M. Farmer, Sample Space for Particle Size and Velocity Measuring Interferometers, Applied Optics, Vol 15, pp 1984-1989, 1976

31. N.S. Hong and A.R. Jones, A Light Scattering Technique for Particle Sizing Based on Laser Fringe Anemometry, J.Phys.D: Appl.Phys., Vol 9, pp 1839-1848, 1976

32. A.R. Jones, A Review of Drop Size Measurement - The Application of Techniques to Dense Fuel Sprays, Proc. Energy Com. Sci, Vol 3, pp 225-234, 1977

33. D.W. Roberds, Particle Sizing Using Laser Interferometry, Appl. Optics, Vol 16, pp 1861-1868, 1977

REFERENCES

34. W.M. Farmer, J.O. Hornkohl, F.A. Swartz and K.E. Harwell, Measurement of Rocket Propellant Exhaust Particles with a Particle Sizing Interferometer, 2nd AIAA/ASME Thermophysics and Heat Transfer Conference, paper 78-918, Palo Alto, CA, May 1978

35. W.D. McComb and S.M. Salih, Comparison of Some Theoretical Concentration Profiles for Solid Particles in a Turbulent Jet with the Results of Measurements Using a Laser-Doppler Anemometer, J. Aerosol Sci, Vol 9, pp 299-313, 1978

36. G. Wigley, The Sizing of Large Droplets by Laser Anemometry, Sci. Instr., Vol 11, pp 639-642, 1978

37. L.B. Thorn, S. Smith, J.W. Connaughton, J.A. Murfree, W.W. Wharton and E. Miller, Propellant Smoke Particle Size Distribution and Concentration Measurements and their Correlation with Condensation Nuclei Theory, 1979 JANNAF Propulsion Meeting, Vol III, pp 279-302, Chemical Propulsion Information Agency Publication 300, 1979

38. W.D. Bachalo, Method for Measuring the Size and Velocity of Spheres by Dual-Beam Light Scatter Interferometry, Applied Optics, Vol 19, pp 363-370, 1980

39. J.D. Knapton and I.C. Stobie, Dynamic Fracture Pressure of Quartz, Ballistic Research Laboratory Technical Note 1712, 1969 (AD 687286)

40. S.M. De Corso, Effect of Ambient and Fuel Pressure on Spray Drop Size, Trans. ASME, Vol 82, Series A, p 10, 1962

41. M. Born and E. Wolf, Principles of Optics, p. 433, Pergamon Press, 1959

42. R. Menzel and F.M. Shofner, An Investigation of Fraunhofer Holography for Velocimetry Applications, Applied Optics, Vol 9, pp 2073-2079, 1970

43. W.M. Farmer, BRL Particle Sizing Interferometer, BRL Contract Report (in preparation), (Contract No. DAAD05-79-C-1004), 1981

REFERENCES

44. Private communications between F. Weinberg, Imperial College, and K.E. Travis and J.D. Knapton, BRL, 1979 and J.D. Knapton 1981

45. R.N. Savage and G.M. Hieftje, Enhancement of Pneumatic Nebulization Efficiency Through Application of an Electric Field, Rev. Sci. Instrum 49, p. 1418-1424, 1978

BIBLIOGRAPHY

A.R. Hanson, E.G. Domich and H.S. Adams, Shock Tube Investigation of the Breakup of Drops by Air Blast, The Physics of Fluids Vol VI, pp 1070-1080, 1963

E. Rabin, A.R. Schallenmuller and R.B. Lawhead, Displacement and Shattering of Propellant Droplets - Final Summary Report, Air Force Office of Scientific Research, Combustion Dynamics Division (Contract AF 18 (603)-98), 1960

APPENDIX A

Critical Weber Numbers for Water and Methyl Alcohol (From Reference 2)

APPENDIX A

Table A1. Critical Weber Numbers for Water and Methyl Alcohol (from Reference 2)

Fluid	v m/s	D μm	W_e crit
water	25.7	600	3.60
water	33.4	410	4.23
water	47.9	270	6.00
water	72.7	120	6.55
methyl alcohol	18.3	625	5.98
methyl alcohol	25.7	330	6.34
methyl alcohol	33.4	230	7.62
methyl alconol	47.9	118	8.41

APPENDIX B

WATER SPRAY TESTS CONDUCTED AT THE UNIVERSITY OF TENNESSEE SPACE INSTITUTE

W. Michael Farmer, Fred A. Schwartz and J. D. Knapton

WATER INJECTION TESTS PERFORMED AT THE UNIVERSITY OF TENNESSEE SPACE INSTITUTE (USTI)

A particle sizing interferometer (PSI) developed at UTSI was used to record droplet data for water jets. A cylindrical container of water was pressurized manually with Nitrogen gas. Injection pressures were limited to the maximum pressure of the gas cylinder at about 12.4 MPa and tests were conducted with injection pressures varying between 12.4 MPa and 9.6 MPa. The water was ejected from a 1.6 mm nozzle with an $l/d = 4.0$. This nozzle was similar to the larger nozzle used in the BRL tests.

Data were recorded during each test in two or three sample size number groups. The groups for each test were recorded sequentially. The volume of water ejected for each test was sufficiently large (test duration was about 2-3 sec) which permitted the recording of two or three groups of data each with a preselected sample size of usually 500.

The numbers recorded by the PSI were consistent for the different groups from each test with the exception of the last group which generally indicated smaller droplet sizes. This discrepancy was likely due to hydraulic flow during the recording of the first one or two groups and pneumatic flow during the last group. The pneumatic flow condition was associated with a gas liquid mixing in the pressure cylinder resulting in both an audible and visual change in the jet characteristics. For this reason the data recorded during the last group are not summarized here. Data obtained during the tests are summarized in Table B1. A combined print out of data from the first four tests is shown in Table B2. A correction for the velocity is necessary on the printout sheets (Table B2) and is obtained by dividing the recorded velocity by the f number*of the imaging lens.

With the exception of Test No. 4-12-80-2, the data in Table B1 suggests a very weak correlation between the volumetric mean diameter and velocity. The volumetric mean diameter decreases by about 10% for a 77% increase in velocity. Test No. 4-12-80-2 yielded a significantly lower mass concentration when compared with the other tests, perhaps due to the jet missing the probe volume.

An examination of the individual diameter velocity data points does not suggest the correlation indicated by a plot (from Table B1) of the volumetric mean diameter and velocity. For example, a plot of the individual diameter and velocity data in Table B3 for Test No. 5-12-80-15 shows for most of the droplets

---

* f number = 5 for test on 5-12-80 and 16 for tests on 4-12-80 (Table B1)

a distribution located between 40 and 120 m/s** with a corresponding droplet diameter between 25 and 85 μm. Interestingly, the plot revealed a grouping of data points at several locations. The groups are summarized in Table B4.

The test also showed that a small precentage of drops were recorded that fall outside of the normal distribution. For example, Table B2 shows that 29 drops were recorded in the totaled histogram with a diameter less than 5.04 μm. This number corresponds to 6.8 % of the total number of accepted events.

** Correct velocities are obtained by dividing by the f number.

TABLE B1. SUMMARY OF TESTS AT UTSI

Test No.	Distance from Jet Nozzle to Probe Volume (mm)	Diameter of Orifice (mm)	Velocity (m/s)	Volumetric Mean (μm)	Mass Concentration (g/m^3)	Number of Accepted Events	Percent of Total Events Accepted (%)
5-12-80-12	432	1.6	16.1	57.2	502	107	21.4
5-12-80-13	432	1.6	13.0	61.6	899	82	16.4
5-12-80-15	432	1.6	15.9	59.1	337	141	28.2
5-12-80-16	432	1.6	12.4	63.9	1350	94	18.8
4-12-80-2	889	1.6	7.4	52.2	0.004	402	92.4
4-12-80-10	889	1.6	9.1	63.4	3.1	68	61.3

TABLE B 2

T O T A L E D D I S T R I B U T I O N H I S T O G R A M S

RUN NUMBERS FOR TOTALED HISTOGRAM
12 13 15 16
12/5/80
WATER SPRAY WITH 0.062 NOZZLE DIAMETER
F#=5 NOZZLE 17" FROM PROBE VOLUME
600 VPMT TRUE FRINGE PERIOD=20.17

TOTAL SAMPLE SIZE = 2000
APERIODICITY ACCEPTED = 551
TOTAL ACQUISITION TIME = 35.01
TOTAL SIZE ACCEPTED = 424
GEOMETRIC MEAN = 45.7 SIGMA G = 44.5
FIRST MOMENT = 53.9 SECOND MOMENT = 3.336E+03
THIRD MOMENT = 2.172E+05 FOURTH MOMENT = 1.465E+07

ARITHMETIC MEAN = 53.9
VOLUME/AREA MEAN = 65.1
VOLUMETRIC MEAN = 60.1
MASS MEAN = 67.5

GAMMA = 2.88 ACCEPTANCE RATIO = .275 KAPPA = .360
NUMBER DENSITY (N/CC) = 5.805E+03 MATERIAL DENSITY = .999
MASS CONCENTRATION (GM/CUBIC METER) = 660. WHEN NL = 10
ALPHA EXTINCTION = 7.5511E-02 SIGMA BAR = 8581.

VISIBILITY CALIBRATION CONSTANTS
EXP = 0 COEFFICIENT = 1.00000E+00

TIME AVERAGED STATISTICS

GEOMETRIC MEAN = 44.9 SIGMA G = 44.5
FIRST MOMENT = 52.9 SECOND MOMENT = 3.188E+03
THIRD MOMENT = 2.012E+05 FOURTH MOMENT = 1.312E+07

ARITHMETIC MEAN = 52.9
VOLUME/AREA MEAN = 63.1
VOLUMETRIC MEAN = 58.6
MASS MEAN = 65.2

MASS CONCENTRATION (GM/CUBIC METER) = 478. WHEN NL = 10
ALPHA EXTINCTION COEFF. SIGMA BAR
7.606605E-02 8004.50

TABLE B 2 (Continued)

RUN NUMBERS FOR TOTALED HISTOGRAM
12 13 15 16
12/5/80
WATER SPRAY WITH 0.062 NOZZLE DIAMETER
F#=5 NOZZLE 17" FROM PROBE VOLUME
600 VPMT TRUE FRINGE PERIOD=20.17

NUMBER DISTRIBUTION

BIN	DIAM	DIFF %	PROBABILITY	WTPOP	WEIGHT	VIS	POP
1	5.04	8.518E-02	8.518E-02	68.7	2.37	.997	29
2	10.08	0.00	8.518E-02	0.00	2.37	.988	0
3	15.13	5.874E-03	9.105E-02	4.74	2.37	.972	2
4	20.17	1.175E-02	.103	9.48	2.37	.951	4
5	25.21	2.056E-02	.123	16.6	2.37	.925	7
6	30.25	2.565E-02	.149	20.7	2.30	.893	9
7	35.30	3.135E-02	.180	25.3	2.30	.856	11
8	40.34	3.593E-02	.216	29.0	2.23	.815	13
9	45.38	6.080E-02	.277	49.1	2.23	.770	22
10	50.42	8.670E-02	.364	70.0	2.12	.722	33
11	55.47	.123	.487	99.6	2.12	.670	47
12	60.51	.136	.623	109.	1.99	.617	55
13	65.55	.133	.756	107.	1.99	.562	54
14	70.60	.103	.859	82.8	1.80	.506	46
15	75.64	7.808E-02	.937	63.0	1.80	.449	35
16	80.68	3.919E-02	.976	31.6	1.02	.393	31
17	85.72	1.419E-02	.990	11.5	.818	.337	14
18	90.76	9.034E-03	.999	7.29	.729	.283	10
19	95.81	8.006E-04	1.000	.646	.323	.231	2
20	100.85	0.00	1.000	0.00	.293	.181	0
21	105.89	0.00	1.000	0.00	.293	0.00	0

MASS DISTRIBUTION

BIN	DIAM	% MASS	PROBABILITY	WTPOP	WEIGHT	VIS	POP
1	5.04	5.028E-05	5.028E-05	68.7	2.37	.997	29
2	10.08	0.00	5.028E-05	0.00	2.37	.988	0
3	15.13	9.362E-05	1.439E-04	4.74	2.37	.972	2
4	20.17	4.438E-04	5.877E-04	9.48	2.37	.951	4
5	25.21	1.517E-03	2.105E-03	16.6	2.37	.925	7
6	30.25	3.271E-03	5.376E-03	20.7	2.30	.893	9
7	35.30	6.348E-03	1.172E-02	25.3	2.30	.856	11
8	40.34	1.086E-02	2.258E-02	29.0	2.23	.815	13
9	45.38	2.616E-02	4.875E-02	49.1	2.23	.770	22
10	50.42	5.118E-02	9.992E-02	70.0	2.12	.722	33
11	55.47	9.702E-02	.197	99.6	2.12	.670	47
12	60.51	.138	.335	109.	1.99	.617	55
13	65.55	.173	.508	107.	1.99	.562	54
14	70.60	.166	.674	82.8	1.80	.506	46
15	75.64	.156	.830	63.0	1.80	.449	35
16	80.68	9.475E-02	.924	31.6	1.02	.393	31
17	85.72	4.116E-02	.966	11.5	.818	.337	14
18	90.76	3.110E-02	.997	7.29	.729	.283	10
19	95.81	3.241E-03	1.000	.646	.323	.231	2
20	100.85	0.00	1.000	0.00	.293	.181	0
21	105.89	0.00	1.000	0.00	.293	0.00	0

TABLE B 2 (Continued)

RUN NUMBERS FOR TOTALED HISTOGRAM
12 13 15 16
12/5/80
WATER SPRAY WITH 0.062 NOZZLE DIAMETER
F#=5 NOZZLE 17" FROM PROBE VOLUME
600 VPMT TRUE FRINGE PERIOD=20.17

NUMERIC SIZE DISTRIBUTION

5.04	8.518E-02	X**********
10.1	0.00	X
15.1	5.874E-03	X**
20.2	1.175E-02	X****
25.2	2.056E-02	X*******
30.3	2.565E-02	X*********
35.3	3.135E-02	X**********
40.3	3.593E-02	X**********
45.4	6.080E-02	X**********
50.4	8.670E-02	X**********
55.5	.123	X**********
60.5	.136	X**********
65.6	.133	X**********
70.6	.103	X**********
75.6	7.808E-02	X**********
80.7	3.919E-02	X**********
85.7	1.419E-02	X*****
90.8	9.034E-03	X***
95.8	3.006E-04	X
101.	0.00	X
106.	0.00	X

MASS DISTRIBUTION

5.04	5.028E-05	X
10.1	0.00	X
15.1	9.362E-05	X
20.2	4.438E-04	X
25.2	1.517E-03	X
30.3	3.271E-03	X
35.3	6.348E-03	X*
40.3	1.086E-02	X***
45.4	2.616E-02	X*******
50.4	5.118E-02	X**********
55.5	9.702E-02	X**********
60.5	.136	X**********
65.6	.173	X**********
70.6	.166	X**********
75.6	.156	X**********
80.7	9.475E-02	X**********
85.7	4.116E-02	X**********
90.8	3.110E-02	X*********
95.8	3.241E-03	X
101.	0.00	X
106.	0.00	X

TABLE B 3

U T S I G A S D I A G N O S T I C S D I V I S I O N

LONG FRINGE COUNT	7	
SHORT FRINGE COUNT	5	
PRECOUNT	1	
CLOCK FREQUENCY	70.00	MHZ
HIGH PASS FILTER	.2000	MHZ
FRINGE PERIOD	100.8	
MAXIMUM APERIODICITY	5.000	%
DC OFFSET	4.900	VOLTS
TIMER RATE	1000.0	HZ
SYSTEM VOLTAGE GAIN	40.0	
SAMPLE SIZE	500	
RUN NUMBER	15	

P R I N T M O D E
A L L M O D E
P A R T I C L E S I Z I N G M O D E
12/5/80
WATER SPRAY WITH 0.062 NOZZLE DIAMETER
F#=5 NOZZLE 17" FROM PROBE VOLUME
600 VPMT TRUE FRINGE PERIOD=20.17

VEL	VIS	SIZE	PED	FR	DOPP	DR	LCC	SCC	TIME
43.8	.740	50.4	.139	1	.103	1	1126	805	15.4
40.2	.671	55.5	6.701E-02	0	4.494E-02	0	1228	839	15.4
166.	.654	60.5	.827	0	.541	0	298	207	15.4
53.0	.738	50.4	.662	1	.489	1	932	669	15.4
59.5	.789	45.4	.141	0	.111	0	831	585	15.4
63.1	.604	65.6	.314	1	.190	0	783	563	15.4
49.7	.707	55.5	2.719E-02	0	1.921E-02	0	995	690	15.4
44.5	.642	60.5	.382	1	.245	1	1110	794	15.4
51.0	.795	45.4	5.854E-02	0	4.657E-02	0	969	701	15.4
84.6	.596	65.6	.127	0	7.541E-02	0	584	405	15.4
127.	.355	85.7	1.87	1	.663	0	388	271	15.4
104.	.651	60.5	.429	0	.279	0	473	339	15.4
87.0	.671	55.5	.513	1	.344	0	568	401	15.4
119.	.576	65.6	.417	0	.240	0	417	294	15.4
58.3	.723	50.4	.151	0	.109	0	847	597	15.4
57.6	.668	60.5	8.548E-02	0	5.712E-02	0	858	636	15.4
69.5	1.230	5.04	1.674E-02	0	2.059E-02	0	711	499	15.4
108.	.575	65.6	.123	0	7.088E-02	0	457	337	15.4
107.	.558	70.6	.325	0	.181	0	460	317	15.4
73.4	.549	70.6	.162	0	8.881E-02	0	673	478	15.4
101.	.657	60.5	.472	0	.310	0	487	345	15.4
83.5	.669	60.5	.167	0	.112	0	592	411	15.4
72.2	.734	50.4	.106	0	7.799E-02	0	684	502	15.4
62.2	.650	60.5	.327	1	.213	1	794	572	15.4
81.1	.725	50.4	.437	1	.317	0	609	432	15.4
112.	.547	70.6	.345	0	.189	0	443	316	15.4
62.5	.443	80.7	.185	0	8.174E-02	0	791	571	15.4
112.	.463	75.6	.113	0	5.244E-02	0	441	315	15.4
112.	.536	70.6	.159	0	8.549E-02	0	443	313	15.4
97.9	.539	70.6	.569	1	.307	0	505	372	15.4
72.9	.575	65.6	.121	0	6.935E-02	0	678	478	15.5
115.	.686	55.5	.337	0	.231	0	430	301	15.5
49.8	.743	50.4	8.022E-02	0	5.957E-02	0	993	716	15.5
40.4	.312	90.8	.163	1	5.102E-02	0	1224	876	15.5
71.8	.714	55.5	6.173E-02	0	4.410E-02	0	688	490	15.5

VEL	VIS	SIZE	PED	PR	DOPP	DR	LCC	SCC	TIME
67.7	.594	65.6	.126	0	7.481E-02	0	730	521	15.5
95.0	.460	75.6	.769	1	.353	0	520	366	15.5
56.4	.875	35.3	.148	0	.129	0	876	626	15.5
51.3	.536	70.6	3.902E-02	0	2.093E-02	0	963	668	15.5
99.4	.670	60.5	.281	0	.189	0	497	352	15.5
100.	.873	35.3	.255	0	.223	0	493	349	15.5
91.7	.479	75.6	.186	0	8.894E-02	0	539	371	15.5
112.	.519	70.6	.943	1	.490	0	442	315	15.5
81.0	.861	35.3	.608	1	.524	1	610	436	15.5
64.3	.576	65.6	8.319E-02	0	4.794E-02	0	769	576	15.5
82.1	.661	60.5	8.640E-02	0	5.711E-02	0	602	431	15.5
87.2	.728	50.4	9.861E-02	0	7.182E-02	0	567	407	15.5
69.9	.438	80.7	5.223E-02	0	2.286E-02	0	707	520	15.5
74.0	.551	70.6	5.121E-02	0	2.822E-02	0	668	458	15.5
55.7	.857	35.3	6.477E-02	0	5.550E-02	0	887	615	15.5
54.7	.722	50.4	.381	1	.275	1	904	639	15.5
26.1	.655	60.5	.178	1	.117	1	1895	1367	15.5
87.3	.961	20.2	2.838E-02	0	2.726E-02	0	566	416	15.5
57.8	.727	50.4	.122	0	8.837E-02	0	855	622	15.5
76.0	.653	60.5	5.182E-02	0	3.384E-02	0	650	469	15.5
113.	.689	55.5	.348	0	.240	0	437	303	15.5
109.	.470	75.6	.901	1	.424	0	455	316	15.5
76.1	.411	80.7	9.018E-02	0	3.706E-02	0	649	458	15.5
115.	.373	85.7	.383	0	.143	0	431	295	15.5
130.	.760	50.4	.233	0	.177	0	380	258	15.5
61.0	.398	80.7	6.824E-02	0	2.717E-02	0	810	554	15.5
60.4	.718	55.5	3.920E-02	0	2.816E-02	0	818	582	15.5
73.9	.670	60.5	.103	0	6.896E-02	0	669	474	15.6
60.0	.563	65.6	4.035E-02	0	2.273E-02	0	824	592	15.6
84.8	.347	85.7	.146	0	5.086E-02	0	583	421	15.6
99.6	.536	70.6	.822	1	.440	0	496	354	15.6
44.4	1.104	5.04	1.809E-02	0	1.993E-02	0	1112	766	15.6
56.1	.676	55.5	5.063E-02	0	3.422E-02	0	881	637	15.6
88.2	.658	60.5	.526	1	.346	0	560	413	15.6
100.	.583	65.6	.234	0	.136	0	493	355	15.6
157.	.695	55.5	.636	0	.442	0	314	220	15.6
46.5	.582	65.6	.105	0	6.130E-02	0	1063	770	15.6
70.9	1.276	5.04	2.672E-02	0	3.411E-02	0	697	495	15.6
57.7	.731	50.4	8.633E-02	0	6.312E-02	0	857	630	15.6
55.0	.669	60.5	9.602E-02	0	6.423E-02	0	898	628	15.6
69.9	.596	65.6	.158	0	9.418E-02	0	707	516	15.6
80.6	1.488	5.04	3.852E-02	0	5.730E-02	0	613	422	15.6
56.7	1.165	5.04	.125	0	.145	0	871	636	15.6
65.9	.928	25.2	.103	0	9.592E-02	0	750	536	15.6
65.7	.605	65.6	.340	1	.205	0	752	518	15.6
63.2	.620	60.5	6.221E-02	0	3.859E-02	0	782	560	15.7
74.2	.716	55.5	5.239E-02	0	3.749E-02	0	666	481	15.7
87.5	.558	70.6	.228	0	.127	0	565	421	15.7
85.9	.506	70.6	.337	0	.170	0	575	422	15.7
108.	.676	55.5	.293	0	.198	0	457	322	15.7
84.3	.655	60.5	.108	0	7.089E-02	0	586	430	15.7
78.6	.579	65.6	8.255E-02	0	4.777E-02	0	629	429	15.7
59.2	.897	30.3	6.010E-02	0	5.388E-02	0	835	615	15.7
78.9	.903	30.3	.114	0	.103	0	626	462	15.7
120.	.594	65.6	.289	0	.172	0	412	280	15.7
99.8	.505	75.6	.422	0	.213	0	495	346	15.7
83.9	.647	60.5	9.302E-02	0	6.017E-02	0	589	412	15.7
66.5	.830	40.3	6.003E-02	0	4.984E-02	0	743	526	15.7
84.6	.552	70.6	.137	0	7.559E-02	0	584	435	15.7
44.8	1.150	5.04	.134	1	.155	1	1102	795	15.7

VEL	VIS	SIZE	PED	PR	DOPP	DR	LCC	SCC	TIME
61.3	.589	65.6	.209	1	.123	0	806	568	15.7
98.4	.681	55.5	.146	0	9.969E-02	0	502	349	15.7
62.6	.576	65.6	8.787E-02	0	5.059E-02	0	789	536	15.8
100.	.926	25.2	5.821E-02	0	5.392E-02	0	494	346	15.8
106.	.454	75.6	.198	0	9.012E-02	0	468	334	15.8
57.6	.411	80.7	.100	0	4.128E-02	0	858	606	15.8
106.	.664	60.5	.232	0	.154	0	466	340	15.8
93.2	.798	45.4	.197	0	.157	0	530	371	15.8
80.5	1.293	5.04	7.687E-02	0	9.940E-02	0	614	430	15.8
75.9	.496	75.6	.119	0	5.907E-02	0	651	466	15.8
68.5	.708	55.5	6.467E-02	0	4.580E-02	0	721	526	15.8
66.0	.472	75.6	9.489E-02	0	4.483E-02	0	749	549	15.8
84.9	.500	75.6	.149	0	7.426E-02	0	582	400	15.8
102.	1.139	5.04	5.204E-02	0	5.926E-02	0	486	332	15.8
103.	.481	75.6	.185	0	8.875E-02	0	478	340	15.8
85.5	.525	70.6	.166	0	8.710E-02	0	578	422	15.8
47.4	.883	35.3	5.336E-02	0	4.709E-02	0	1043	720	15.8
82.9	.775	45.4	.236	0	.183	0	596	405	15.8
129.	.502	75.6	.175	0	8.772E-02	0	382	271	15.8
55.8	1.063	5.04	2.306E-02	0	2.451E-02	0	865	646	15.8
63.0	.735	50.4	.182	0	.134	0	784	568	15.8
115.	.576	65.6	.255	0	.147	0	430	313	15.8
36.6	1.214	5.04	.146	1	.177	1	1349	969	15.9
88.4	.608	65.6	.133	0	8.097E-02	0	559	399	15.9
107.	.696	55.5	.145	0	.101	0	463	327	15.9
51.4	.724	50.4	9.958E-02	0	7.209E-02	0	961	658	15.9
60.2	.684	55.5	.141	0	9.624E-02	0	821	602	15.9
109.	.531	70.6	.997	1	.530	0	455	332	15.9
91.7	.563	65.6	.347	0	.195	0	539	386	15.9
97.7	.385	85.7	.176	0	6.775E-02	0	506	367	15.9
41.2	.801	45.4	.171	1	.137	1	1199	889	15.9
51.4	1.151	5.04	1.286E-02	0	1.480E-02	0	962	715	15.9
111.	.619	60.5	4.900E-02	0	3.034E-02	0	444	303	15.9
57.1	.888	35.3	8.322E-02	0	7.387E-02	0	865	646	15.9
82.4	.306	90.8	.203	0	6.214E-02	0	600	421	15.9
77.3	1.026	5.04	5.925E-02	0	6.079E-02	0	639	477	15.9
92.2	.543	70.6	.106	0	5.757E-02	0	536	373	15.9
70.7	.420	80.7	.167	0	7.002E-02	0	699	495	15.9

TABLE B4 GROUPING OF DATA POINTS FROM TEST NO. 5-12-80-15

Velocity m/s ± %	Particle Size µm - µm	Number of Data Points in Group
11.2 + 1.8 - 1.6	30.2 - 35.3	4
11.7 + 8.1 - 6.6	45.4 - 50.4	5
13.0 + 7.9 - 8.0	60.5 - 65.5	7
16.9 + 4.5 - 2.7	55.5 - 60.5	5
17.5 + 5.4 - 3.3	65.5 - 70.6	6
22.1 + 1.4 - 3.1	65.5 - 70.6	5

LISTS OF SYMBOLS AND ABBREVIATIONS

C	Constant
d	diameter
D	droplet diameter
l	length of injection orifice
L	jet breakup length
LP	HAN-based liquid monopropellant
L_p	Laplace number
NOS	Naval Ordnance Station
O_e	Ohnesorge number
p	pressure
r	radius
R_e	Reynolds number
T	temperature
W	mass flow rate
W_e	Weber number
v	jet velocity
ρ	density
σ	surface tension
τ	wall shear
μ	viscosity

subscripts

c	critical
d	discharge
g	gas
i	injection
j	jet
l	liquid

DISTRIBUTION LIST

No. of Copies	Organization
12	Administrator Defense Technical Info Center ATTN: DTIC-DDA Cameron Station Alexandria, VA 22314
1	Director Defense Advanced Research Projects Agency ATTN: H. Fair 1400 Wilson Boulevard Arlington, VA 22209
1	HQDA (DAMA, C. Church) Washington, DC 20310
1	Commander US Army Materiel Development and Readiness Command ATTN: DRCDMD-ST 5001 Eisenhower Avenue Alexandria, VA 22333
5	Commander US Army Armament Research and Development Command ATTN: DRDAR-TSS (2) DRDAR-SCA, M. Devine D. Adams B. Brodman Dover, NJ 07801
4	Commander US Army Armament Research and Development Command ATTN: DRDAR-LCA, D. Downs A. Beardell DRDAR-LCE, N. Slagg DRDAR-LCS, W. Quine Dover, NJ 07801
1	Commander US Army Armament Research and Development Command ATTN: DRDAR-TDC (Dr. D. Gyorog) Dover, NJ 07801
2	Commander US Army Armament Research and Development Command Benet Weapons Laboratory ATTN: DRDAR-LCB-TL P. Votis Watervliet, NY 12189
1	Commander US Army Armament Materiel Readiness Command ATTN: DRSAR-LEP-L, Tech Lib Rock Island, IL 61299
1	Commander US Army Aviation Research and Development Command ATTN: DRDAV-E 4300 Goodfellow Blvd. St. Louis, MC 63120
1	Director US Army Air Mobility Research and Development Laboratory Ames Research Center Moffett Field, CA 94035
1	Commander US Army Communications Research and Development Command ATTN: DRDCO-PPA-SA Fort Monmouth, NJ 07703
1	Commander US Army Electronics Research and Development Command Technical Support Activity ATTN: DELSD-L Fort Monmouth, NJ 07703
1	Commander US Army Harry Diamond Labs ATTN: DELHD-TA-L 2800 Powder Mill Road Adelphi, MD 20783

DISTRIBUTION LIST

No. of Copies	Organization
1	Commander US Army Missile Command ATTN: DRSMI-R Redstone Arsenal, AL 35898
1	Commander US Army Missle Command ATTN: DRSMI-YDL Redstone Arsenal, Al 35898
2	Commander US Army Mobility Equipment Research and Development Cmd ATTN: DRDME-WC DRSME-RZT Fort Belvoir, VA 22060
1	Commander US Army Tank Automotive Research and Development Cmd ATTN: DRDTA-UL Warren, MI 48090
1	Commander US Army Research Office ATTN: R. Singleton P.O. Box 12211 Research Triangle Park, NC 27709
1	Director US Army TRADOC Systems Analysis Activity ATTN: ATAA-SL, Tech Lib White Sands Missile Range NM 88002
1	Chief of Naval Operations Dept of the Navy ATTN: Code NOP-351G Washington, DC 20350
1	Commander Naval Sea Systems Command ATTN: J.W. Murrin (SEA-62R) National Center Building 2, Room 6E08 Washington, DC 20362
1	Commander Naval Surface Weapons Center Dahlgren, VA 22448
2	Commander Naval Surface Weapons Center ATTN: O. Dengel K. Thorsted Silver Spring, MD 20910
2	Commander Naval Weapons Center ATTN: C. Mallory S. Wood China Lake, CA 93555
2	Commander Naval Ordnance Laboratory ATTN: K. Mueller G. Poudrier Indian Head, MD 20640
1	Superintendent Naval Postgraduate School Monterey, CA 93940
2	AFATL/ATWG, O. Heiney DLD, D. Davis Eglin, AFB, FL 32542
1	AFOSR/NA (L. Caveny) Bldg. 410 Bolling AFB, DC 20332
2	US Bureau of Mines ATTN: R.A. Watson 4800 Forbes Avenue Pittsburgh, PA 15213
1	Director Los Alamos National Laboratory ATTN: T. D. Butler P.O. Box 1663, MS B216 Los Alamos, NM 87545

DISTRIBUTION LIST

No. of Copies	Organization
1	Director Jet Propulsion Laboratory ATTN: Tech Lib 4800 Oak Grove Drive Pasadena, CA 91103
2	Director National Aeronautics and Space Administration ATTN: MS-603, Tech Lib MS-86, Dr. Povinelli Lewis Research Center 21000 Brookpark Road Cleveland, OH 44135
1	Director National Aeronautics and Space Administration Manned Spacecraft Center Houston, TX 77058
1	The BDM Corporation ATTN: Dr. T.P. Goddard P.O. Box 2019 2600 Cearden Road Monterey, CA 93940
1	Calspan Corporation ATTN: E. Fisher P.O. Box 400 Buffalo, NY 14225
1	Food & Machinery Corporation Northern Ordnance Division ATTN: J. Oberg Columbia Heights Post Office Minneapolis, MN 55421
3	General Electric Ordnance Dpt ATTN: J. Mandzy R.E. Mayer H. West 100 Plastics Avenue Pittsfield, MA 01203
2	General Electric Company Armanent Systems Department ATTN: E. Ashley M. Bulman Burlington, VT 05401
1	Pulsepower Systems, Inc. ATTN: L.C. Elmore 815 American Street San Carlos, CA 93555
1	AFELM, The Rand Corporation ATTN: Library D 1700 Main Street Santa Monica, CA 90406
1	Science Applications, Inc. ATTN: R. Edelman 23146 Cumorah Crest Woodland Hills, CA 91364
1	Shock Hydrodynamics ATTN: W. Anderson 4710-16 Vineland Ave. N. Hollywood, CA 91602
1	TRW Systems ATTN: R11032, E. Fishman One Space Park Redondo Beach, CA 90278
1	Director Applied Physics Laboratory The Johns Hopkins University Johns Hopkins Road Laurel, MD 20707
2	Director Chemical Propulsion Information Agency The Johns Hopkins University ATTN: T. Christian Tech Lib Johns Hopkins Road Laurel, MD 20707

DISTRIBUTION LIST

No. of Copies	Organization
1	Pennsylvania State University Dept. of Mechnical Engineering ATTN: K. Kuo University Park, PA 16802
2	Princeton Combustion Research Laboratories ATTN: N.A. Messina M. Summerfield 1041 US Highway One North Princeton, NJ 08540
1	SRI International ATTN: Code L3106, G.A. Branch 333 Ravenswood Avenue Menlo Park, CA 94025

Aberdeen Proving Ground

Dir, USAMSAA
ATTN: DRXSY-D
DRXSY-MP, H. Cohen
Cdr, USATECOM
ATTN: DRSTE-TO-F
Dir, USACSL, Bldg. E3516, EA
ATTN: DRDAR-CLB-PA

USER EVALUATION OF REPORT

Please take a few minutes to answer the questions below; tear out this sheet, fold as indicated, staple or tape closed, and place in the mail. Your comments will provide us with information for improving future reports.

1. BRL Report Number _____

2. Does this report satisfy a need? (Comment on purpose, related project, or other area of interest for which report will be used.)

_____

_____

_____

3. How, specifically, is the report being used? (Information source, design data or procedure, management procedure, source of ideas, etc.) _____

_____

_____

4. Has the information in this report led to any quantitative savings as far as man-hours/contract dollars saved, operating costs avoided, efficiencies achieved, etc.? If so, please elaborate.

_____

_____

5. General Comments (Indicate what you think should be changed to make this report and future reports of this type more responsive to your needs, more usable, improve readability, etc.) _____

_____

_____

_____

6. If you would like to be contacted by the personnel who prepared this report to raise specific questions or discuss the topic, please fill in the following information.

Name: _____

Telephone Number: _____

Organization Address: _____

_____

_____

FOLD HERE

Director
US Army Ballistic Research Laboratory
Aberdeen Proving Ground, MD 21005

NO POSTAGE
NECESSARY
IF MAILED
IN THE
UNITED STATES

OFFICIAL BUSINESS
PENALTY FOR PRIVATE USE, $300

BUSINESS REPLY MAIL
FIRST CLASS PERMIT NO 12062 WASHINGTON, DC
POSTAGE WILL BE PAID BY DEPARTMENT OF THE ARMY

Director
US Army Ballistic Research Laboratory
ATTN: DRDAR-TSB-S
Aberdeen Proving Ground, MD 21005

FOLD HERE

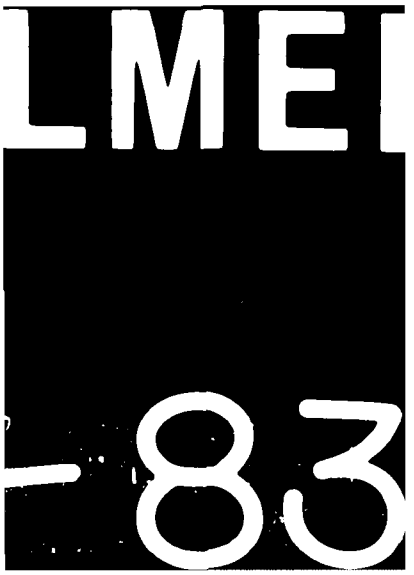
LME
83